Regionalized protein localization domains in the hair cell kinocilium.

Timothy Erickson[1, *], William Paul Biggers III[2], Kevin Williams[2], and Alexandra Venuto[2]

[1] Department of Biology, University of New Brunswick, Fredericton, NB E3B 5A3, Canada

[2] Department of Biology, East Carolina University, Greenville, NC 27858, USA

*Correspondence: timothy.erickson@unb.ca

Abstract

Sensory hair cells are the receptors for auditory, vestibular, and lateral line sensory organs in vertebrates. These cells are distinguished by "hair"-like projections from their apical surface collectively known as the hair bundle. Along with the staircase arrangement of actin-filled stereocilia, the hair bundle features a single, non-motile, true cilium called the kinocilium. The kinocilium plays important roles in hair bundle development and the mechanics of sensory detection. To understand more about kinocilial development and structure, we performed a transcriptomic analysis of zebrafish hair cells looking for cilia-associated genes that have yet to be characterized in hair cells. Here, we focus on three such genes - *ankef1a*, *odf3l2a*, and *saxo2* - because the human or mouse orthologs are either associated with sensorineural hearing loss or are located near uncharacterized deafness loci. We made transgenic fish that express fluorescently tagged versions of their proteins, demonstrating their localization to the kinocilia of zebrafish hair cells. Furthermore, we find that Ankef1a, Odf3l2a, and Saxo2 exhibit distinct localization patterns along the length of the kinocilium. Lastly, we report a novel overexpression phenotype for Saxo2. Overall, these results suggest that the hair cell kinocilium is regionalized along its proximal-distal axis and set the groundwork to understand the role of these kinocilial proteins in hair cell structure and function.

Keywords:

hair cells; kinocilium; cilia; deafness; hearing loss; lateral line; transcriptomics; TU-tagging; zebrafish; ANKEF1; ODF3L2; SAXO2

1. Introduction

Our senses of hearing and balance rely on the function of sensory receptors in our ears called hair cells. Sensory hair cells are distinguished by hair-like projections from their apical surface that detect and transduce physical stimuli such as sound waves or head movements. Most of these projections are actin-filled microvilli (called stereocilia) that form the characteristic stair-cased hair bundle. However, at some point in their development, all vertebrate hair cells also feature a single microtubule-based projection called the kinocilium.

Cilia play prominent roles in sensory cell development and function from an evolutionarily diverse set of organisms [1,2]. In mechanosensory hair cells, the kinocilium can fulfil both sensory and structural roles, depending on the type of hair cell. Although kinocilia degenerate around the onset of hearing in mammalian cochlear hair cells, they nonetheless play a developmental role in establishing hair bundle polarity in the auditory system [3] and mediating Sonic Hedgehog signaling to instruct cochlear development [4,5]. In contrast to the transient kinocilia of cochlear hair cells, the kinocilium is a permanent and prominent feature of most other vertebrate hair cells in the auditory, vestibular, and lateral line organs, including vestibular hair cells of mammals. In non-cochlear cells, it appears that kinocilia play a less pronounced role in establishing bundle polarity. However, they contribute to the structure and functional mechanics of the sensory hair bundle [6–8], as well as act as attachment points for inert masses such as otoliths and otoconia [9]. Kinocilial dynamics may also be involved in the repair and regeneration of cochlear hair cells [10]. As such, it is fundamental to our understanding of sensory hair cells to characterize the structural and functional components of the kinocilium.

Hair cell kinocilia possess several features that distinguish them from both non-motile, primary cilia and from motile cilia and flagella. Although "kino-" means "motion" and kinocilia usually possess the "9+2" arrangement of axonemal microtubules typically found in motile cilia [11], the hair cell cilium is non-motile, lacking the inner dynein arms and nexin links found in motile cilia [12]. In this respect, kinocilia are similar to some mammalian olfactory cilia, which also have a 9+2 axoneme but lack the dynein machinery to generate motion [13]. However, given the impressive diversity of vertebrate hair cells, it is possible that active movement is a feature of some kinocilia [14,15]. In some contexts, non-"9+2" arrangements of microtubules have also been reported [10,12]. Like hair cells themselves, there is great diversity in kinocilial morphology - from the transient kinocilia of cochlear hair cells, to the bulbed kinocilia of amphibian hair cells, to the towering kinocilia of superficial lateral line neuromasts (and everything in between). However, little is known about the molecular bases for this diversity.

Sensorineural hearing loss can result from mutations in cilia-associated genes as part of a syndromic ciliopathy, such as reported for Alström, Bardet-Biedl, and Usher syndromes [16–18]. Cilia- and microtubule associated genes are also implicated in nonsyndromic hearing loss, examples being *CCDC50* [19], *MAP1B* [20], and *DCDC2* [21]. *PCDH15* and *CDH23* are also examples of cilia-associated Usher proteins where certain alleles result in nonsyndromic hearing loss [22,23]. There may be other cilia-associated genes waiting to be identified that contribute to auditory and / or vestibular function.

To characterize putative kinocilial genes, we have turned to the zebrafish model system. Zebrafish hair cells are genetically and molecularly related to mammalian hair cells [24]. This allows us to utilize the genetic tractability of zebrafish to characterize protein localization and function for putative human deafness genes. Here, we identify hair cell-enriched transcripts by TU-tagging and focus on three putative kinocilial genes within the dataset - *ankef1a*, *odf3l2a*, and *saxo2* - because of their potential involvement in hearing loss. Mouse *Ankef1* lies within the coloboma (*Cm*) deletion locus whose phenotypes include auditory and vestibular deficits [25,26]. The Shared Harvard Inner Ear Database (SHIELD) reports that human *ODF3L2* and *SAXO2* lie within deafness loci DFNB72 and DFNA30, respectively [27]. We have made transgenic fish that express tagged Ankef1a, Odf3l2a, and Saxo2 proteins and demonstrate their distinct localization patterns within the kinocilium of zebrafish hair cells. Our results set the groundwork for future studies to understand the role of these kinocilial proteins in hair cell structure and function.

2. Methods

2.1. Animal husbandry

Adult zebrafish were maintained and bred using standard procedures [28]. Larval fish were grown at 28.5ºC on a 14:10 hour light cycle in 100 mm Petri dishes containing E3 media (5 mM NaCl, 0.17 mM KCl, 0.33 mM CaCl2 and 0.33 mM MgSO4 buffered with NaHCO3).

2.2. Transgenic fish lines

The *Tg(myo6b:actb1-EGFP)vo8* and *Tg(myo6b:yfp-Hsa.TUBA)idc16* transgenic lines have been previously described [8,29] and were gifts from the lab of Teresa Nicolson. For the TU-tagging experiments, we used a *Tg(myo6b:HA-UPRT-P2A-NLS-mCherry)* line that was similar to, but distinct from, the *Tg(HA-UPRT-P2A-mCherry)* line used previously [30]. The *Tg(myo6b:ankef1a-emGFP)unb4*, *Tg(myo6b:odf3l2a-emGFP)unb5*, *Tg(myo6b:saxo2-emGFP)unb6*, and *Tg(myo6b:saxo2-mKate2)unb7* lines were generated for this study. For the sake of simplicity, we refer to these lines as Ankef1a-GFP, Odf3l2a-GFP, Saxo2-GFP, and Saxo2-mKate2 throughout the manuscript. Coding sequences were amplified using total RNA from 7 days post-fertilization (dpf) zebrafish using the SuperScript IV One-step RT-PCR kit (ThermoFisher) using the primers listed in Table S1. Entry and Destination constructs were made using standard Tol2 Gateway cloning protocols [31].

2.3. Thiouracil (TU)-tagging and bioinformatics

The TU-tagging experiments were performed essentially as previously described [30] with the following modifications. Transgenic and wild type sibling larvae from outcrosses of a *Tg(myo6b:HA-UPRT-P2A-NLS-mCherry)* (abbreviated *Tg(UPRT)*) line were used. Stock solutions of 4-thiouracil (4TU; Sigma-Aldrich 440736) and 4-thiouridine (4sU; Sigma-Aldrich T4509) were prepared at 0.5 M and 0.25 M, respectively in DMSO (Sigma-Aldrich D8418). Working solutions were diluted in E3 media with a final DMSO concentration of 0.5%. At 4 dpf, *Tg(UPRT)* larvae were treated with 2 mM 4TU while non-transgenic siblings were treated with 1 mM 4sU. Both groups were bathed in their respective compounds for 3.5 hours at 29ºC. The conversion of 4TU to 4-thiouridine monophosphate is enhanced in the presence of the *Toxoplasma gondii* UPRT enzyme while

117 endogenous biosynthetic pathways can make 4-thiouridine monophosphate directly from
118 4sU. With this strategy, TU-tagged RNA is preferentially synthesized in the hair cells of
119 *Tg(UPRT)* larvae treated with 4TU while RNA is tagged without bias for cell type in 4sU-
120 treated, non-transgenic controls. The experiment was performed in biological duplicate
121 where a biological sample is defined as 100 larvae per treatment group produced by a single
122 breeding event.

123 Samples were processed according to the manufacturer's protocol in TRIzol reagent
124 (Ambion 15596026) and enriched for polyadenylated mRNA using the Dynabeads
125 Oligo(dT)25 kit (Ambion 61005). Biotinylation of the mRNA was done using the MTSEA-
126 biotin-XX reagent (Biotium 90066). A 5 mg/ml solution was prepared in *N,N*-
127 Dimethylformamide (DMF; Sigma-Aldrich 227056). A 10X biotinylation buffer was
128 prepared by diluting 1 M Tris-HCl pH 7.5 (ThermoFisher 15567027) to 100 mM and 0.5
129 M EDTA pH 8 (ThermoFisher AM9261) to 10 mM in nuclease-free water (ThermoFisher
130 AM9930). The biotinylation reaction was performed by heating the mRNA in a 1X
131 biotinylation buffer solution at 65ºC for 2 minutes before adding 10 µg of MTSEA-biotin-
132 XX solution with a final DMF concentration of 25%. Samples were incubated in the dark
133 at room temperature for 30 minutes on a rotating rack. mRNA was recovered by adding an
134 equal volume of chloroform:isoamyl alcohol 24:1 (Sigma-Aldrich C0549), vortexing,
135 retrieving the aqueous phase with 5Prime Phase Lock Gel (Heavy) microfuge tubes, and
136 performing a NaCl-isopropanol precipitation with glycogen (ThermoFisher R0551) acting
137 as an inert carrier. Biotinylated RNA was fragmented to approximately 200 – 500 bases
138 with the NEBNext Magnesium RNA Fragmentation Module (New England Biolabs
139 E6150S) and precipitated by adding 1/10 volume of 3M sodium acetate pH 5.5
140 (ThermoFisher AM9740) plus 3 volumes of 100% ethanol, again with glycogen as an inert
141 carrier. Finally, biotinylated TU-tagged RNA was separated from untagged RNA using the
142 µMacs Streptavidin kit (Miltenyi Biotec 130-074-101). High salt MPG buffer (100 mM
143 Tris, 10 mM EDTA, 1 M NaCl, 0.1% Tween-20) and 100 mM dithiothreitol (DTT; Sigma-
144 Aldrich 3860-OP) were prepared fresh. RNA samples (50 ul) were heated to 65ºC for 5
145 minutes and iced. Resuspended µMass beads (100 µl) were added and samples were
146 incubated for 15 minutes in the dark at room temperature with rotation. µMacs columns
147 were equilibrated with 2 x 100 µl of nucleic acid buffer (supplied with kit) before applying
148 the RNA-bead samples to the columns. Columns were washed with twice with 65ºC MPG
149 buffer and twice with room temperature buffer. TU-tagged RNA was eluted from each
150 column with 2 x 100 µl 100 mM DTT heated to 65 ºC. Eluted RNA was recovered by
151 NaOAc - ethanol precipitation as above, resulting in two biological samples of hair cell
152 enriched, TU-tagged RNA from Tg(UPRT) larvae treated with 4TU and two biological
153 samples of tagged RNA from non-transgenic larvae treated with 4sU.

154 RNA-seq library construction and sequencing was done by the OHSU Massively
155 Parallel Sequencing Shared Resource (Oregon Health & Science University, Portland OR).
156 The raw RNA-seq data was imported into an OHSU instance of the Galaxy platform [32]
157 and mapped to the *Danio rerio* GRCz10 genome. The resulting BAM files were imported
158 to SeqMonk (https://www.bioinformatics.babraham.ac.uk/projects/seqmonk/) for data
159 visualization and statistical analysis using default parameters for DESeq2. Transcripts that
160 were significantly enriched in the *Tg(UPRT)* samples were analyzed for GO biological
161 process term enrichment using the Panther database [33,34]. Analysis of *ODF3L2* and
162 *SAXO2* genomic positions relative to known deafness loci was done using information

from the Hereditary Hearing Loss website [35] and by searching the GRCh38.p13 human genome assembly through Ensembl [36] for the loci-defining genetic markers described in the relevant publications.

2.4. Whole mount mRNA in situ hybridization

mRNA in situ hybridizations *odf3l2a* and *saxo2* were performed as described [30]. Probe templates were amplified using primers listed in Table S1. The *odf3l2a* template was amplified from total RNA with T3 and T7 sites on the forward and reverse primers respectively and the DIG-labeled antisense probe was synthesized directly from purified PCR product using T7 RNA polymerase (NEB M0251S). The *saxo2* probe templates were amplified from total RNA with gene specific primers and cloned into the pCR4-TOPO vector (Thermo Fisher 450071) for use as the template for DIG-labeled probe synthesis. *saxo2* plasmids were linearized with PmeI before synthesizing the DIG-labeled antisense probe with T7 RNA polymerase.

2.5. Confocal microscopy, image analysis, and statistics

Live zebrafish larvae (5 – 7 dpf) were anesthetized in 0.016% MS-222 and mounted in 1.2% low-melting point agarose overlaid with E3 media containing MS-222. Confocal imaging was performed with a Zeiss LSM 700 confocal microscope equipped with a 40X water immersion objective. Pixel intensity and kinocilium length analyses were done in Fiji [37] and the "cool" lookup table was used to encode pixel intensity in maximum Z-projections. Neuromast images in Figure 2E-H contain "choppiness" artifacts produced by rotation of 3D Z-projections. Images were compiled and adjusted for brightness and contrast in Adobe Photoshop CC.

Length measurements for lateral cristae kinocilia were done by tracing a kinocilium from base to tip through a confocal Z-stack using the SNT plugin for ImageJ [38,39] and calculating the Euclidean distance for kinocilial length by Pythagorean theorem. The transmitted light channel was used to define the start and end of each kinocilium. A single biological sample (n) is defined as the per larva average of the five tallest kinocilia that could be unambiguously traced. Per larva averages were used for statistical comparisons between transgenic larvae and non-transgenic siblings.

Fluorescent protein distributions along the length of lateral crista kinocilia were quantified in ImageJ using the "plot profile" function with a segmented line width setting of "2". 16-bit pixel intensity values were recorded every 0.064 µm. Measurable kinocilia were defined as having a minimum length of 32 µm and for which the intensity profile could be unambiguously measured from base to distal tip using the transmitted light channel as a guide. To account for differences in kinocilial length, pixel intensity values were registered to the most distal measurement of each kinocilium, meaning that proximal intensity values for kinocilia that are longer than 32 µm are not included in the intensity profile measurement analysis. Pixel intensity values at each position were averaged from all measured kinocilia to create an average gray value over a distance of 32 µm. To account for differences in overall fluorescence levels between transgenes, the average gray values were rescaled using min-max normalization to a 0-100 scale and plotted as log2 values fit with a loess curve.

RNA sequencing data were visualized and plotted using Seqmonk (https://www.bioinformatics.babraham.ac.uk/projects/seqmonk/) and analyzed using default Seqmonk settings for DESeq2. Statistical tests for kinocilial length were performed in R Studio [40] using the base R stats package [41] for Welch two-sided t-tests and the ANOVA. Plots were generated with ggplot2 [42].

3. Results

3.1. Identification of putative kinocilia-associated, hair cell-enriched transcripts.

Thiouracil (TU) tagging is a method for purifying mRNA transcripts from specific cell types [43]. To identify genes expressed in sensory hair cells (Figure 1A), we performed TU-tagged RNA-seq experiments on larval zebrafish, introducing several protocol changes relative to our previous study (See Methods) [30]. We identified 1838 features that are significantly enriched in the 4TU-treated *Tg(UPRT)* sample vs. the 4sU-treated wild type controls (Figure 1B). See Table S2 for the full list of significantly TU-enriched genes from this study. Gene Ontology (GO) enrichment analysis of 1675 uniquely mapped features reveals that genes associated with hearing, hair cells, and inner ear development are statistically overrepresented in the TU-enriched dataset (Table S3), confirming that the experiment successfully enriched for hair cell transcripts. There is also a significant enrichment of genes associated with microtubule-and cilium-based processes (Table S4), highlighting genes with potential roles in the structure and / or function of kinocilia.

Next, we manually searched the entire TU-enriched dataset for putative kinocilial genes that may be associated with deafness phenotypes in mice and humans, but whose protein products have not been previously localized to the kinocilium. For this study, we focus on three such genes - *ankef1a*, *odf3l2a*, and *saxo2*. *ankef1a* expression in zebrafish hair cells has been previously reported [44]. Here, we confirm enriched hair cell expression for *odf3l2a* and *saxo2* by mRNA in situ hybridization on 3 days post-fertilization (dpf) larvae. *odf3l2a* expression is restricted to inner ear and lateral line hair cells (Figure 1C), consistent with the pattern reported for the *et10.4* enhancer trap line where the transgenic insertion is 1.5 kilobases (kb) upstream of the *odf3l2a* gene [45]. *saxo2* is also expressed in otic and lateral line hair cells, with additional robust expression in the developing olfactory epithelia (Figure 1D).

3.2. Evaluation of ANKEF1, ODF3L2, and SAXO2 as potential human deafness genes.

Ankyrin repeat and EF-hand domain containing 1 (ANKEF1) is predicted to contain protein-protein interaction (ankyrin) and calcium-sensing/binding (EF-hand) domains. Functionally, *Ankef1* has been implicated in *Xenopus* gastrulation and fertility in male mice [46,47]. ANKEF1 protein localization to the cilium has not been demonstrated, but transcriptomic and proteomic analyses suggest it is enriched in ciliated cells (including mouse and zebrafish hair cells) [44,48–55].

Human *ANKEF1* is on chromosome 20 (GRCh38: 20:10034987-10058303) and not located near any known human deafness loci [35] (Table 1). However, the mouse *Ankef1* ortholog is located within the coloboma (*Cm*) deletion locus [56,57]. *Cm* heterozygotes exhibit morphological abnormalities in the organ of Corti and head bobbing indicative of vestibular defects [26,58]. Most of these *Cm* phenotypes can be attributed to the heterozygous loss of the Notch ligand Jagged 1 (*Jag1*). However, the authors note that the

Cm and *Jag1* mutant phenotypes are not equivalent and speculate that other genes within deletion may contribute to the inner ear defects in *Cm* mutants [26].

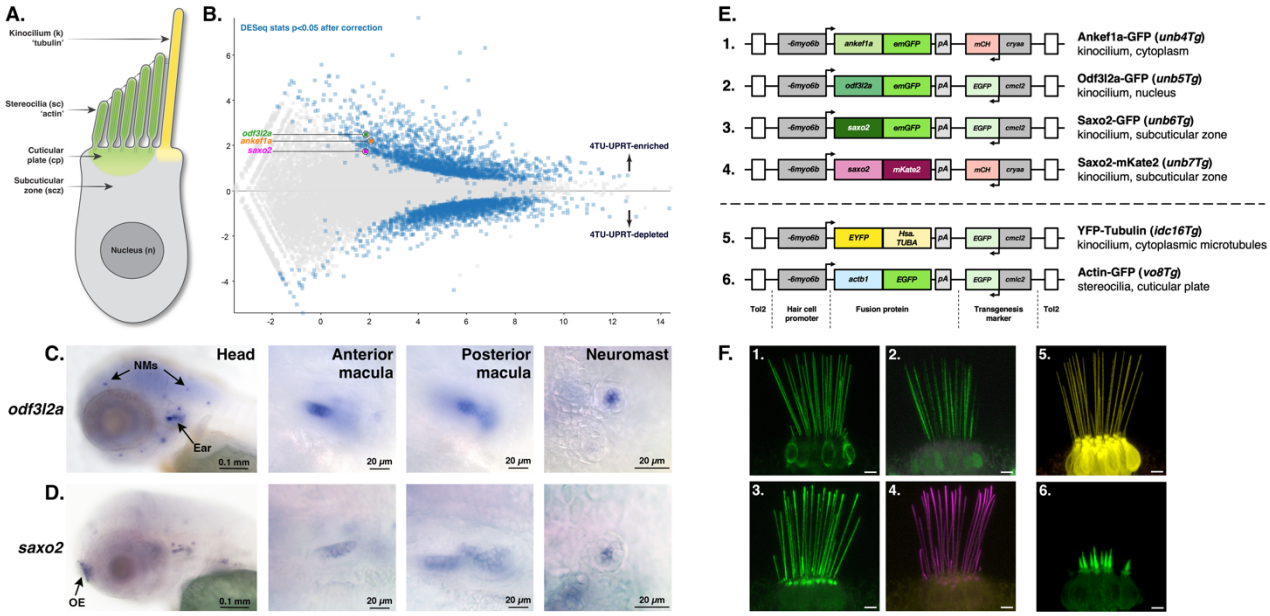

Figure 1. Identification of cilium-associated genes with enriched expression in zebrafish hair cells. **A.** Diagram of a generic sensory hair cell. **B.** Scatter plot of differentially expressed genes identified by TU-tagging. *ankef1a*, *odf3l2a*, and *saxo2* are indicated in the 4TU-UPRT-enriched population. **C, D.** mRNA in situ hybridization (ISH) for *odf3l2a* and *saxo2* in 3 days post-fertilization (dpf) zebrafish larvae. NMs = neuromasts; oe = olfactory epithelium **E.** Schematics of transgenes used in this study. **F.** Overview of Ankef1a-GFP (1), Odf3l2a-GFP (2), Saxo2-GFP (3), Saxo2-mKate2 (4), YFP-TUBA (5), and Actb1-GFP (6) protein localization in the lateral cristae of larval zebrafish. Scale bars are 5 µm in F.

Outer dense fiber protein 3-like 2 (ODF3L2) is a member of the ODF3 family of proteins which are characterized by sperm-tail PG (proline-glycine)-rich (STPGR) repeat domains. Note that although ODF families 1-4 share a common nomenclature and associate with microtubule-based structures, these four ODF families are not evolutionarily related to one another. ODF3 (SHIPPO1) was first identified as a component of the outer dense fibers (ODFs) of mouse sperm tails [59]. However, *Odf3* family genes are also expressed in ciliated cells that lack outer dense fibers [60–63], suggesting a broader role in microtubule-based structures [64]. Consistent with this idea, an Odf3l2 homolog in *Giardia* forms part of the basal body proteome [65] and human ODF3L2 can localize to cytoplasmic microtubules in a heterologous expression system [66]. However, ODF3L2 localization to the cilium has not been demonstrated. Functionally, little is known about ODF3 and ODF3L proteins in any cell type. Zebrafish *odf3l2a* is a hair cell-enriched transcript [55] and, although evidence for *Odf3l2* expression in mammalian hair cells is weak, *Odf3l2* knockout mice display high frequency hearing loss and vestibular dysfunction [67]. The underlying cellular causes for these phenotypes are unknown.

Human *ODF3L2* is located on chromosome 19p13.3 (GRCh38:19:463346-474880) (Table 1). The 19p13 region is home to several hearing loss loci, including *DFNB15/72/95*

(*GIPC3*) [68,69], *DFNB68* (*S1PR2*) [70], *DFNB81* / Perrault syndrome (*CLPP*) [68,71], as well as the autosomal dominant *DNFA57* locus (gene unknown) [72]. The *DFNB72* critical region was mapped between markers D19S216 and D19S1034 (GRCh38:19:4949401-6113471) [73]. Although the Shared Harvard Inner-Ear Database (SHIELD) [27] reports that *ODF3L2* is located within the *DFNB72* critical region, the GRCh38 human genome assembly places *ODF3L2* at least 4.4 MB away from the closest *DFNB72* marker D19S216. The *DFNA57* critical region was mapped between markers D19S912 and D19S212 (GRCh38:19:7806762:18232460). *ODF3L2* is almost 7 MB away from the closest marker D19S592 and over 9 MB away from the maximum LOD score marker D19S586. However, the telomeric boundary was defined from a single patient and the authors acknowledge an unlikely possibility that the *DFNA57* interval extends to the telomere. If this is the case, *ODF3L2* remains as a candidate gene for *DFNA57*.

Stabilizer of axonemal microtubules 2 (SAXO2 / FAM154B) is the second of two SAXO family members that are part of the microtubule associated protein 6 (MAP6) family [74,75]. SAXO proteins can stabilize microtubules and use their "Mn" repeat domains to associate with basal bodies, centrioles, and cilia [75–78]. Interestingly, SAXO and MAP6 are MIPs (microtubule inner proteins), meaning they reside in the luminal space of microtubules [79–82]. Furthermore, luminal MAP6 can stabilize microtubule curvature [83], though it is unknown whether SAXO proteins also share this functionality. *Saxo2* is enriched in hair cell transcriptomic datasets from mice and zebrafish [53,55,84] but has not been functionally characterized.

Human *SAXO2* is located on 15q25.2 (Table 1), near several sensorineural deafness loci including *DFNA30* (gene unknown) [85], *DFNA68* (*HOMER*) [86,87], *DFNB48* (*CIB2*) [88,89], and *OTSC1* [90]. SHIELD reports that *SAXO2* maps to the *DFNA30* locus. The critical region for *DFNA30* lies between markers D15S151 and D15S130 (GRCh38:15:87053920-94168232) with a maximum LOD score for marker D15S1004 [85]. However, current genomic coordinates for *SAXO2* (GRCh38:15:82262818-82284927) place it outside the *DFNA30* critical interval, 4.8 MB away from the closest marker D15S151 and 11.5 MB away from D15S1004.

Table 1: Human *ANKEF1*, *ODF3L2*, and *SAXO2* chromosomal locations compared to potential associated deafness loci.

Human gene	Cytogenetic Location	GRCh38.p13 coordinates	Proposed deafness locus	Critical region markers	Locus coordinates	Causative gene	Reference
ANKEF1	20p12.2	20:10034987-10058303	n/a	n/a	n/a	n/a	n/a
ODF3L2	19p13.3	19:463346-474880	*DFNB72*	D19S216 - D19S1034	19:4949401-6113471	*GIPC3*	Ain et al. [73]
			DFNA57	D19S912 - D19S212	19:7806762 - 18232460	unknown	Bönsch et al. [72]
SAXO2	15q25.2	15:82262818-82284927	*DFNA30*	D15S151 - D15S130	15:87053920-94168232	unknown	Mangino et al. [73]

298 *3.3. Distinct localization patterns of Ankef1a, Odf3l2a, and Saxo2 proteins in the hair cell*
299 *kinocilium.*

300 To analyze the subcellular localization of Ankef1a, Odf3l2a, and Saxo2 in zebrafish
301 hair cells, we created stable transgenic fish expressing fluorescently-tagged versions of
302 these proteins under control of the hair cell-specific *myo6b* promoter (Figure 1E). Tagged
303 Ankef1a, Odf3l2a, and Saxo2 proteins all exhibit robust localization to the hair cell
304 kinocilium (Figure 1F).

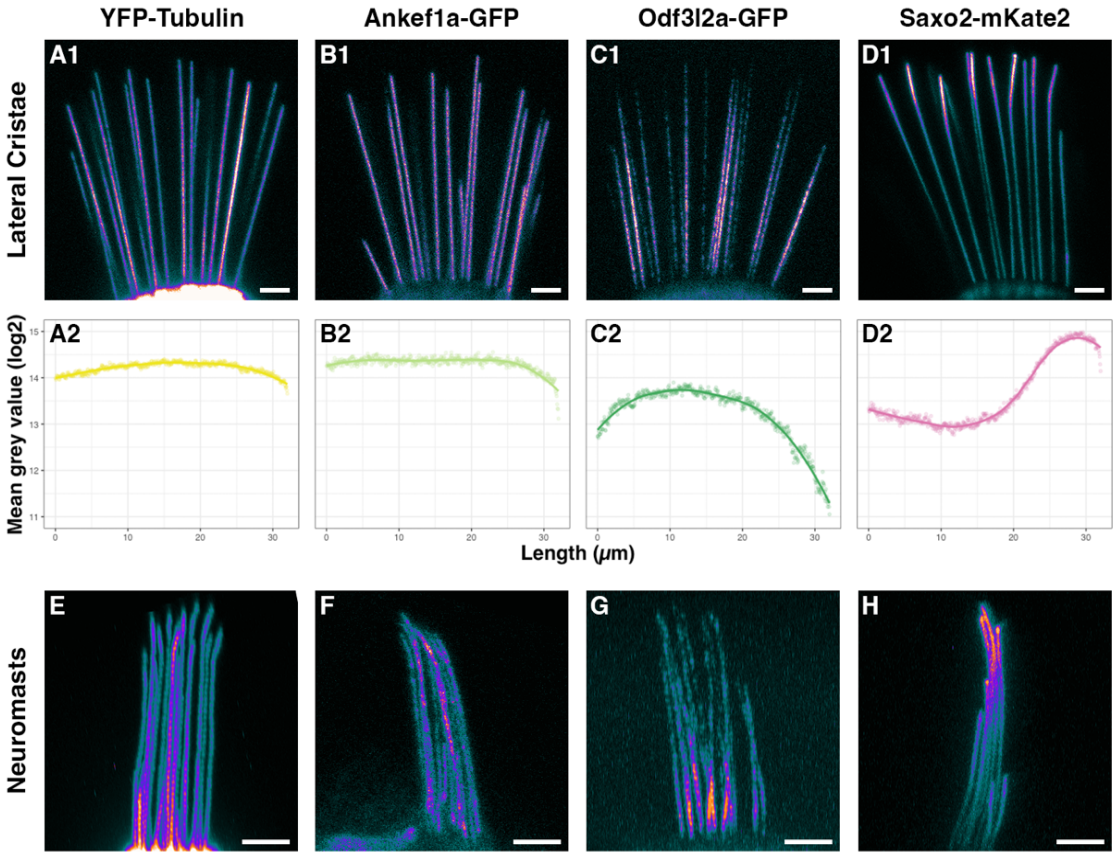

Figure 2. Distributions of tubulin, Ankef1a, Odf3l2a, and Saxo2 in the hair cell kinocilium. **A1 – D1.** Pixel intensity-encoded images of tagged tubulin, Ankef1a, Odf3l2a, and Saxo2 proteins in the kinocilia of lateral cristae hair cells. Brighter colours indicate higher fluorescence intensity. **A2 – D2.** Scatter plots of mean grey values (log2) for fluorescence intensity from kinocilia in the lateral cristae. YFP-TUBA: n = 35 kinocilia from 8 individuals; Ankef1a-GFP: n = 23 from 8 individuals; Odf3l2a-GFP: n = 30 from 11 individuals; Saxo2-mKate2: n = 17 from 6 individuals. Position 0 µm is from the proximal region near the base of kinocilia and position 32 µm is the distal-most tip. **E – H.** Pixel intensity-encoded images of neuromast kinocilia from zebrafish larvae expressing YFP-TUBA (E), Ankef1a-GFP (F), Odf3l2a-GFP (G), or Saxo2-mKate2 (H). Scale bars are 5 µm in panels A1-D1, E-H.

305 We imaged the lateral cristae and neuromasts of live larvae at 5 – 6 dpf and encoded
306 differences in pixel intensity by applying the ImageJ "cool" lookup table to maximum z-
307 projections (Figure 2A1-D1, E-H). We also quantified fluorescence intensity in these
308 kinocilia and present the average fluorescence intensity distribution as a log2 mean grey
309 value over the most distal 32 µm (Figure 2A2-D2). For comparison, we also used the

Tg(myo6b:yfp-Hsa.TUBA)idc16 line that expresses YFP-tagged alpha tubulin in hair cells, marking both cytoplasmic and axonemal microtubules as well as a pool of unpolymerized tubulin. As expected, YFP-TUBA is uniformly distributed along the length of the hair cell kinocilium in the lateral cristae and neuromasts (Figure 2A1, A2, E). Ankef1a-GFP displays a similarly uniform distribution from base to tip (Figure 2B1, B2, F). The distribution of Odf3l2a-GFP is distinct from that of tubulin and Ankef1a, with Odf3l2a being more restricted to the middle-proximal region of the kinocilium (Figure 2C1, C2, G). The distribution of Saxo2-mKate2 is complementary to that of Odf3l2a, with enriched localization to the distal region of the kinocilium and a depletion in the middle-proximal zone (Figure 2D1, D2, H). Interestingly, we observe bent kinocilia in the lateral cristae of Saxo2-mKate2 transgenics (Figure 2D1), a phenotype we do not observe in the other transgenic lines or in non-transgenic siblings. Saxo2-GFP is also enriched in the distal region (Figure S1A, B), but we do not observe kinocilial curvature in this line. Together, these transgenes demonstrate that Ankef1a, Odf3l2a, and Saxo2 are cilia-associated proteins and reveal distinct distribution patterns for each of these proteins in the kinocilia of zebrafish hair cells.

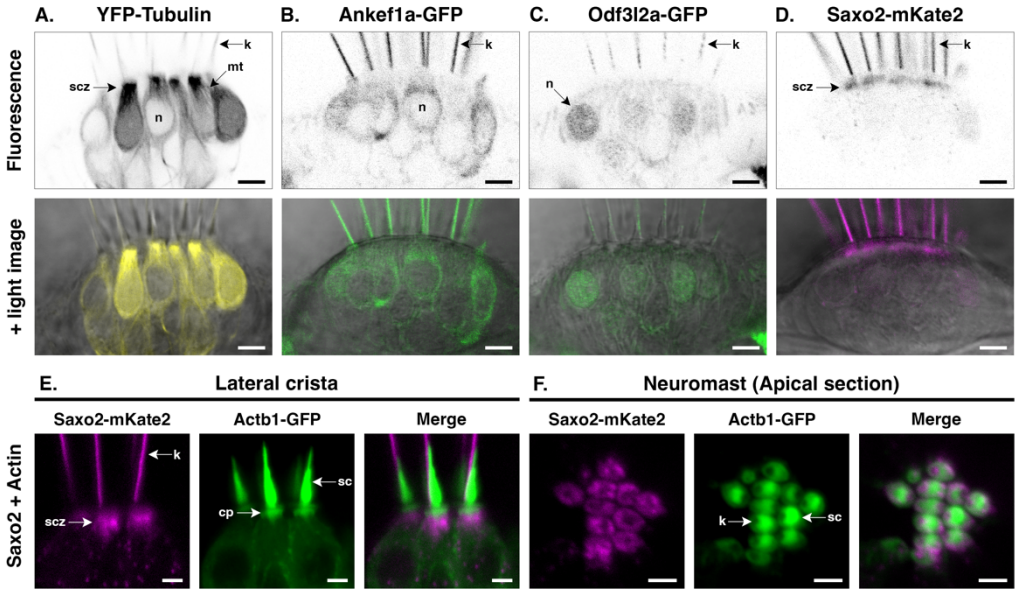

Figure 3. Distinct protein localization patterns in the hair cell soma. **A – D.** Details of YFP-TUBA, Ankef1a-GFP, Odf3l2a-GFP, and Saxo2-mKate2 in the cell body of lateral cristae hair cells. Top panels are black and white representations of the fluorescence channel and lower panels are fluorescence with the corresponding light image. **E, F.** Saxo2-mKate2 (magenta) accumulations in apical part of the hair cell body in cristae and neuromasts. GFP-tagged beta actin is shown in green. scz = subcuticular zone; mt = microtubule; k = kinocilium; n = nucleus; cp = cuticular plate; sc = stereocilia. Scale bars are 5 µm in A – D and 2.5 µm in E and F.

3.4. Ankef1a, Odf3l2a, and Saxo2 exhibit unique distribution patterns in the hair cell soma that are distinct from tubulin.

To determine if Ankef1a, Odf3l2a, and Saxo2 also associate with cytoplasmic tubulin, we compared the cytoplasmic distributions of these three transgenes to that of YFP-TUBA in the soma of hair cells in the lateral crista (Figure 3). In the cytoplasm, the YFP-TUBA signal is strongest in the apical subcuticular zone that lies just below the actin-

rich cuticular plate. Cytoplasmic microtubules are also evident (Figure 3A). Ankef1a-GFP is largely excluded from the subcuticular zone and there is no obvious association with cytoplasmic microtubules (Figure 3B). Instead, the Ankef1a-GFP signal is diffuse throughout the perinuclear cytoplasm. In contrast to Ankef1a, Odf3l2a-GFP signal is mostly absent from the cytoplasm, instead accumulating in the nucleus of some hair cells. In neuromast hair cells, Ankef1a and Odf3l2a display similar localization patterns as in the crista (Figure S2A, B). Lastly, Saxo2-mKate2 does not associate with cytoplasmic microtubules and instead accumulates in the subcuticular zone beneath the apical cuticular plate, marked here by GFP-tagged beta actin (Figure 3D-F). Saxo2-GFP displays a similar apical accumulation in the cell body (Figure 1F, S1A). In top-down views of neuromast hair cells, Saxo2-mKate2 accumulates in rings around the cuticular plate (Figure 3F). In summary, although Ankef1a, Odf3l2a, and Saxo2 all co-localize with tubulin in the kinocilium, none of these proteins share the same distribution pattern as YFP-TUBA in the hair cell soma, nor do their patterns overlap with one another.

3.5. Saxo2-mKate2 overexpression results in curved, truncated, and 'bulbed' kinocilia.

Next, we measured kinocilial height in the lateral crista to determine whether overexpression of Ankef1a, Odf3l2a, or Saxo2 influences kinocilial morphology. The average maximum heights of kinocilia in *YFP-TUBA*, *ankef1a-GFP*, and *odf3l2a-GFP* transgenics were statistically indistinguishable from their non-transgenic siblings (Figure 4A). In contrast to these single transgenic lines, we identified at least three independent lines for Saxo2-mKate2 which we categorize as "mild", "intermediate", and "severe" in terms of their kinocilial phenotypes (Figure 4B-E). A one-way ANOVA comparing the three Saxo2-mKate2 phenotypes and non-transgenic siblings reveals significant differences in kinocilial length ($F_{3,24}$ = 193.3, p < 2e-16). Compared to non-transgenic siblings, maximum height is not affected in "mild" *saxo2-mKate2* transgenics, despite examples of curved kinocilia (Figure 4A-C; non-Tg, n = 8, mean = 35.4 µm; "mild", n = 8, mean = 35.3 µm; *padj* = 0.9858). However, both the "intermediate" and "severe" phenotypes have significantly shorter kinocilia compared to non-transgenic siblings (Figure 4A, D, E; "intermediate", n = 7 mean = 32.1 µm, *padj* < 0.0001; "severe", n = 5, mean = 26.1 µm, *padj* < 0.0001). Transgenics with the "intermediate" phenotype exhibit kinocilial curvature and bulbed tips marked by an accumulation of Saxo2-mKate2 (Figure 4D). Lastly, the "severe" Saxo2-mKate2 phenotype includes a further reduction in average maximum kinocilia height and increased prominence of bulbed tips (Figure 4E). The severe phenotype is also marked by a punctate accumulation of Saxo2-mKate2 in the cell bodies and along the kinocilia. Some of these puncta are bidirectionally mobile in the kinocilia (Video S1). Neuromasts from the severely affected larvae display a similar phenotype (Figure S3). Surprisingly, these "severe" Saxo2-mKate transgenics are viable and qualitatively do not exhibit obvious auditory or vestibular phenotypes as larvae or adults. The Saxo2-GFP line does not exhibit curved kinocilia nor a significant change in kinocilial height (t = -1.8712, df = 5.5674, p-value = 0.1143) (Figure S1C). In summary, transgenic expression of Ankef1a and Odf3l2a does not affect kinocilial height. This is also true of the Saxo2-mKate2 line with lower levels of expression though curved kinocilia are common. Lines with elevated Saxo2-mKate2 levels exhibit bulbed and truncated kinocilia.

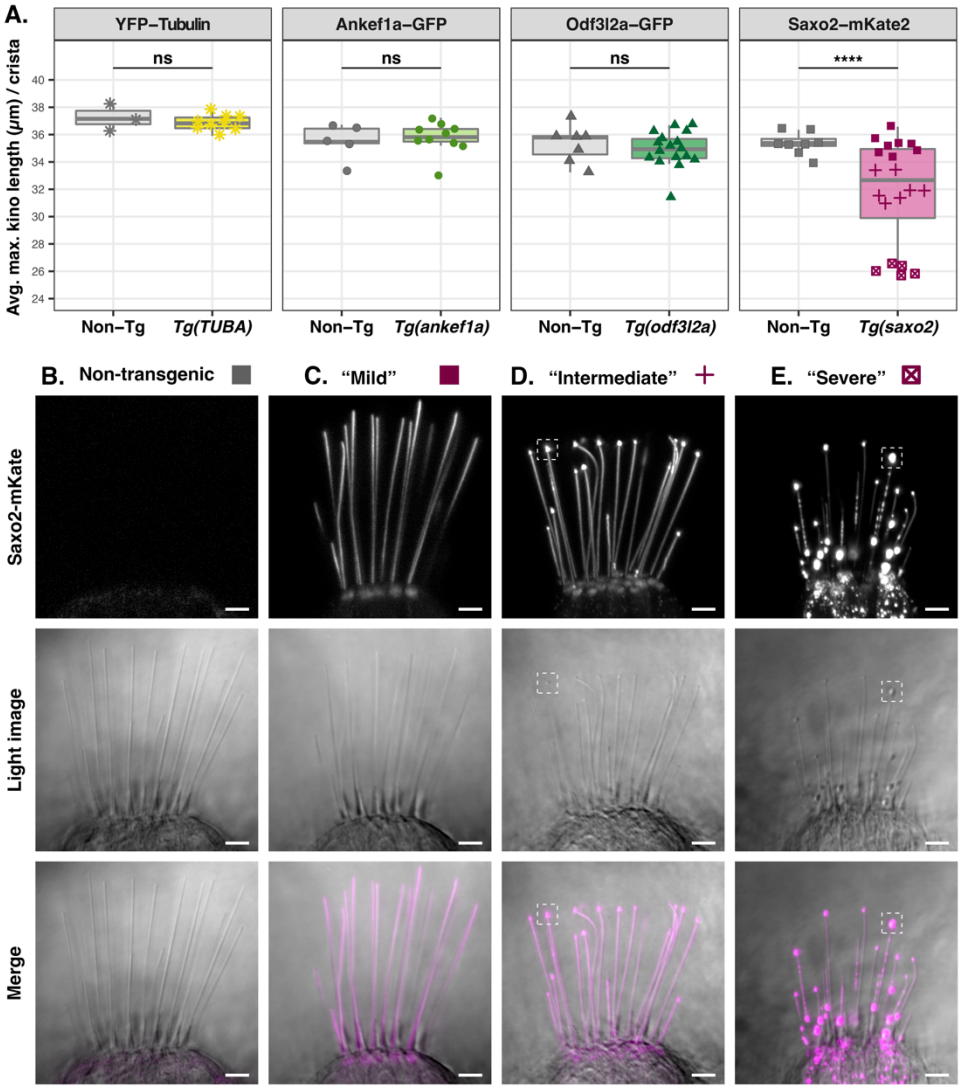

Figure 4. Effect of tubulin, Ankef1a, Odf3l2a, and Saxo2 overexpression on kinocilial length and morphology. **A.** Boxplots of maximum kinocilia length in the lateral crista of *YFP-TUBA*, *ankef1a-GFP*, *odf3l2a-GFP*, and *saxo2-mKate2* transgenics and their non-transgenic siblings. Data points are the average length of the five tallest kinocilia from an individual larva. Based on their morphological phenotypes, the Saxo2-mKate2 data points are grouped as "mild" (solid squares), "intermediate" (crosses), and "severe" (boxed x's). Two-tailed Welch's t-test statistics – YFP-tubulin (6 dpf): non-Tg, n = 3 larvae, mean = 37.3 µm; *Tg(TUBA)*, n = 9, mean = 36.9 µm; t = 0.67757, df = 2.5116, p = 0.5551. Ankef1a-GFP (5 dpf): non-Tg, n = 5, mean = 35.5 µm; *Tg(ankef1a)*, n = 10, mean = 35.7 µm; t = 0.41384, df = 7.079, p = 0.6912. Odf3l2a-GFP (5 dpf): non-Tg, n = 7, mean = 35.3 µm; *Tg(odf3l2a)*, n = 17, mean = 35.0 µm; t = 0.5913, df = 10.931, p = 0.5663. Saxo2-mKate2 (5 dpf) one-way ANOVA ($F_{3,24}$ = 193.3, p < 2e-16). See text for results of pairwise comparisons between the Saxo2-mKate2 phenotypes. **B - E.** Representative images of lateral cristae from non-transgenic (B) and *saxo2-mKate2* transgenics categorized as "mild" (C), "intermediate" (D), and "severe" (E). The dashed boxes in D and E highlight examples of the "bulbed" kinocilial phenotype. ns = not significant; **** = p < 0.00001. Scale bars are 5 µm.

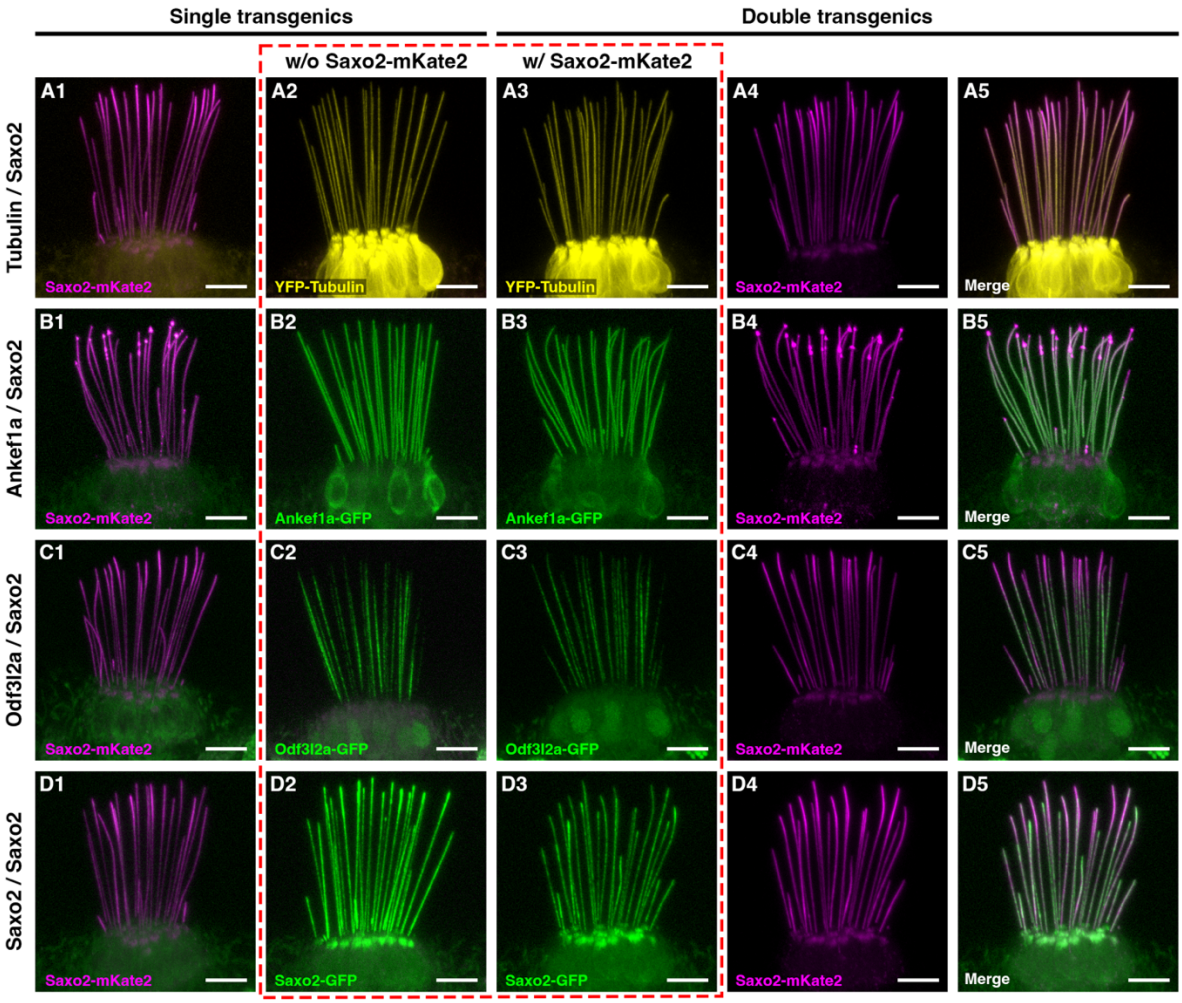

Figure 5. Co-expression of Saxo2-mKate2 with YFP-tubulin (**A**), Ankef1a-GFP (**B**), Odf3l2a-GFP (**C**), and Saxo2-GFP (**D**). Column 1 and 2 of each row shows single transgenic siblings while columns 3 and 4 show individual channels from a double transgenic larva. Column 5 shows the merged channels from columns 3 and 4. The dashed red box compares YFP-TUBA, Ankef1a-GFP, Odf3l2a-GFP, and Saxo2-GFP localization without (A2-D2) or with (A3-D3) the presence of Saxo2-mKate2. Scale bars are 5 µm in all panels.

3.6. Ankef1a, Odf3l2a, and Tubulin distribution patterns are not influenced by Saxo2.

Given that Saxo2-mKate2 can alter kinocilial morphology, we next tested whether the presence of Saxo2-mKate2 influences the distributions of YFP-TUBA, Ankef1a-GFP, Odf3l2a-GFP, and Saxo2-GFP. We produced four combinations of double transgenic fish, each with Saxo2-mKate2 as a common factor. Co-expression of Saxo2-mKate2 with YFP-TUBA (Figure 5A1-5, Figure S4), Ankef1a-GFP (Figure 5B1-5), or Odf3l2a-GFP (Figure 5C1-5) did not alter the distribution patterns of either pair of proteins relative to single transgenic siblings. An example of the Saxo2-mKate2 ”intermediate” phenotype is shown in panels B1, B3-5 while the “mild” phenotype is shown in the other examples. On the other hand, rather than simply overlap with one another, co-expression of Saxo2-mKate

388 and Saxo2-GFP reveals a form of competition for space between these two transgenic
389 proteins (Figure 5D1-5). Most obviously at the tips, either the mKate2 or GFP version of
390 Saxo2 is more abundant with Saxo2-mKate2 appearing to outcompete Saxo2-GFP at the
391 tips of most kinocilia. Taken together, these data suggest that Saxo2 does not positively or
392 negatively influence the distributions of tubulin, Ankef1a, or Odf3l2a in the kinocilium.

393 # 4. Discussion

394 *4.1. Utility of TU-tagging to identify hair cell transcripts.*

395 As with our previously published work [30], here we show that hair cell-enriched
396 transcripts can be identified by thiouracil tagging of newly synthesized RNA. GO analysis
397 confirms that hair cell transcripts are overrepresented in the TU-tagged samples. We also
398 identified all of the TU-enriched transcripts from our previously report, although some
399 gene identifiers from GRCz10 are no longer part of the current GRCz11 genome assembly
400 (*stereocilin-like* genes ENSDARG00000078845 and ENSDARG00000088059, *fam188b2*
401 ENSDARG00000069867, uncharacterized gene ENSDARG00000088304). Changes to
402 the experimental protocol greatly increased the number of significantly enriched genes in
403 the TU-tagged samples. However, in addition to an enrichment of genes related to hair cells
404 and cilia, this dataset is also enriched for genes involved in electron transport and ATP
405 synthesis, iron metabolism, and visual system development and function (Table S2). These
406 results confirm the signal-to-noise problem that seems inherit to TU-tagging in zebrafish.
407 Unless one's experiment requires time resolved differentiation between nascent and
408 preexisting pools of RNA, recent advances in single cell RNA sequencing have largely
409 rendered more error-prone techniques like TU-tagging obsolete.

410 *4.2. Determining the subcellular localization for putative kinocilial proteins.*

411 GFP-tagged proteins have long been valuable tools for live imaging of protein
412 localization [91,92]. This technique has proven particularly invaluable in the analysis of
413 protein localization and function in zebrafish hair cells [8,93–102]. GFP-tagging has also
414 been used extensively to assay for protein localization to microtubules and cilia [66,103–
415 106], including in hair cells [107]. MAP6 family members have also been studied in
416 cultured cells and in vitro using fluorescent protein tags, including MAP6-GFP
417 [83,108,109], and SAXO1- and SAXO2-GFP [76,77]. Importantly, the GFP-tag does not
418 seem to interfere with normal function or localization of cilia-associated proteins. MAP6-
419 GFP and endogenous MAP6 display similar enrichment in the proximal part of neuronal
420 axons [110], and GFP-tagged versions of the Eps15 homology domain proteins EHD1 and
421 EHD3 exhibit the same restricted localization to the proximal part of the primary cilium as
422 the endogenous protein [111]. Thus, GFP-tagging of cilial proteins is a powerful tool for
423 analyzing protein localization in live cells.

424 *4.3. Regionalization of the hair cell kinocilium.*

425 Primary cilia are compartmentalized along their proximal-distal axis into functional
426 domains marked by distinct protein compositions [112]. However, regionalization of the
427 hair cell kinocilium has received little attention. Here, we express tagged versions of hair
428 cell-enriched proteins Ankef1a, Odf3l2a, and Saxo2 in zebrafish to demonstrate their
429 localization to the kinocilium of hair cells. Live imaging of these transgenic proteins also
430 reveals their unique kinocilial localization patterns (Figure 6). Like YFP-tagged tubulin,

Ankef1a-GFP is uniformly distributed along the entire length of the kinocilium. Interestingly, Odf3l2a and Saxo2 exhibit somewhat complementary localization patterns, with Odf3l2a being restricted to the proximal-middle region and Saxo2 accumulating at the kinocilial tips. Together, our study is the first to demonstrate cilial localization for these proteins in hair cells and suggests the existence of regionalized protein localization domains within the kinocilium. It remains to be tested whether these domains are important for kinocilial structure and the sensory function of hair cells.

Based on our results, we propose that Ankef1a, Odf3l2a, and Saxo2 represent three examples of proteins with distinct kinocilial localization or retention signals. Similar to how tubulin monomers line up in an orderly fashion, Ankef1a may contain a "queue-up" motif that prevents accumulation once all available spots are filled, assuring that Ankef1a is evenly distributed along the axoneme. Odf3l2a may encode a "stop" signal that restricts localization to the middle-proximal compartment. Lastly, Saxo2 may contain a "keep walking" signal that allows the protein to accumulate at the plus ends of the axonemal microtubules. These putative localization or sorting motifs may interact with subunits of the IFT machinery and / or with components of the transition zone or axoneme to produce these three distinct kinocilial localization patterns. Our results lay the foundation for future structure-function experiments to understand how these proteins are targeted to cilia and, together with loss-of-function models, to characterize their functional domains.

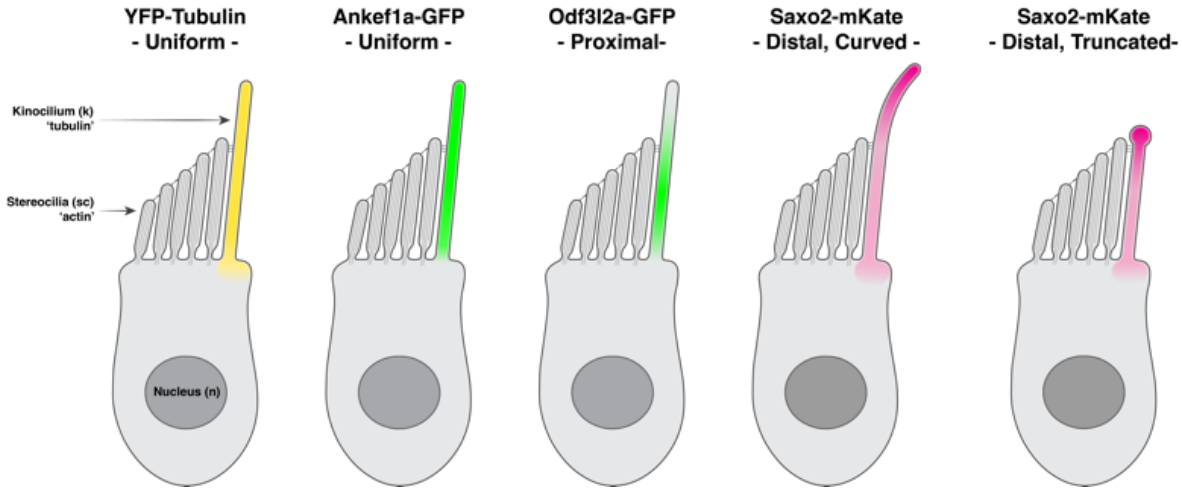

Figure 6. Summary of kinocilial localization patterns and phenotypes for Ankef1a, Odf3l2a, and Saxo2.

4.4. Saxo2 promotes formation of curved and truncated kinocilia.

Kinocilial length and morphology are normal in our *ankef1a* and *odf3l2a* transgenics. However, we find that Saxo2-mKate2 overexpression promotes the formation of curved kinocilia. SAXO proteins are members of the microtubule associated protein 6 (MAP6) family that stabilize microtubules in axons, cilia, and flagella [75,76]. Recent work shows that MAP6 and SAXO are microtubule inner proteins (MIPs) that can localize to the intraluminal space of microtubules [79–81,83]. Full length MAP6 can bind to either the outside or inside of microtubules, and intraluminal localization requires a N-terminal cysteine-rich domain [83]. Luminal MAP6 can stabilize the formation of curved or helical microtubules, a property that externally-bound MAP6 does not possess [83]. Saxo2 also

460 features the cysteine-rich N-terminal domain of the MAP6 family [77]. Given that only
461 luminal MAP6 induces microtubule curvature, it is likely that overexpressed Saxo2 also
462 uses its N-terminal domain to localize to the luminal space of the axonemal microtubules
463 in hair cells. Whether endogenous Saxo2 is a bona fide MIP in the kinocilium remains to
464 be determined. However, our TU-tagging dataset is also significantly enriched for other
465 known MIPs [113], including cilia and flagella associated proteins (Cfap20, 45, and 52),
466 EF-hand domain containing (Efhc) proteins 1 and 2, meiosis-specific nuclear structural 1
467 (Mns1), and Tektins 1-3 (Tables S2, S4). There are likely to be additional hair cell-enriched
468 MIPs and these data suggest a role for intraluminal microtubule associated proteins in our
469 senses of hearing and balance.

470 Saxo2 overexpression also promotes formation of bulbed kinocilia marked by an
471 accumulation of Saxo2 at the tip. This distal accumulation is not accompanied with a
472 concomitant redistribution of Ankef1a, Odf3l2a, or tubulin (Figure S4, Figure 5). This is
473 unlike the kinocilial bulb of bullfrog hair cells that labels strongly for beta tubulin [114].
474 Thus, it is likely that the "canonical" and Saxo2-induced bulbs form by different
475 mechanisms. We also report that Saxo2 overexpression promotes formation of truncated
476 kinocilia and that higher levels of Saxo2 expression are correlated with more severe
477 truncations (Figure 4). This correlation suggests that excess Saxo2 is commandeering the
478 intraflagellar transport (IFT) machinery, leading to Saxo2 accumulation at the tip, possibly
479 at the expense of other components required for normal growth of the kinocilium.
480 However, kinocilial length is unchanged in Saxo2 transgenics with more modest levels of
481 expression (Saxo2-mKate2 "mild" and Saxo2-GFP). Our results differ from those of
482 Dacheux et al. who reported that SAXO1 overexpression almost doubles the length of the
483 primary cilium in cultured RPE1 cells [76]. This discrepancy could be due to differences
484 between the SAXO proteins and / or cell types. We also note differences between the
485 Saxo2-GFP and Saxo2-mKate2 phenotypes. Although the tip-enriched distribution
486 patterns are similar between the two forms, we do not observe curvature or truncation of
487 kinocilia in the Saxo2-GFP line (Figure S1). However, as the Saxo2-mKate2 phenotype
488 intensifies with higher expression levels, we suspect that the comparatively lower levels of
489 Saxo2-GFP expression is the reason for the phenotypic discrepancy between the two tags.
490 There is also reason to believe that the mKate2 version of Saxo2 is trafficked more
491 efficiently to the kinocilium – we observe a greater accumulation of Saxo2-GFP in the
492 subcuticular zone relative to Saxo2-mKate2 and Saxo2-mKate2 tends to accumulate at the
493 tips to the partial exclusion of Saxo2-GFP when they are co-expressed (Figure 5). Although
494 the formation of bulbed and truncated kinocilia is likely an artifact of Saxo2
495 overexpression, the cellular phenotype is nonetheless interesting for its lack of a
496 behavioural correlate. The adult viability and qualitatively normal behaviour of the severe
497 Saxo2 phenotype suggests that a partial loss of normal kinocilial morphology is tolerated
498 under laboratory settings. This tolerance and possible genetic redundancy may account for
499 why hair cell-enriched kinocilial genes have not been identified in genetic screens based
500 on specific auditory or vestibular behavioural phenotypes [115].

501 *4.5. ANKEF1, ODF3L2, and SAXO2 as putative hearing loss genes.*

502 Although we and others have identified many genes that may contribute to form and
503 function of the hair cell kinocilium, we focused on *ankef1a*, *odf3l2a*, and *saxo2* for this
504 study based on preliminary reports of their genetic location in relation to mouse and human

deafness loci. Mouse *Ankef1* is within the coloboma (*Cm*) deletion locus, phenotypes of which include planar polarity defects in the cochlear epithelium, supernumerary hair cells, and hearing and balance defects [25,26]. Deletion of the Notch ligand gene *Jag1* is responsible for the majority of these hearing-related phenotypes, but phenotypical differences between *Cm* and *Jag1* heterozygotes leave open the possibility that other genes in the *Cm* locus are contributing to the phenotype. Since ANKEF1 is a kinocilial protein and Notch pathway mutants display polarity defects indicative of mispositioned kinocilia [116,117], it is possible that the combined heterozygous loss of *Jag1* and *Ankef1* reveals a subtle role for ANKEF1 in kinocilial development which would not be apparent otherwise. Since ANKEF1 has protein-protein interaction Ankyrin repeats and calcium-sensing EF hand domains, one may speculate that ANKEF1 mediates protein-protein interactions in the kinocilium in response to changes in calcium concentrations.

A targeted knockout of *Odf3l2* in mice results in high frequency hearing loss and vestibular deficits [67,118,119]. The cellular basis for these phenotypes is unclear as mouse *Odf3l2* is not robustly expressed in either cochlear or vestibular hair cells [48,84,120]. However, *Odf3l2* expression is detected in outer pillar cells [120,121], suggesting a non-hair cell basis for the mutant phenotype. Interestingly, the homologous *Odf3b* is strongly expressed in mammalian hair cells, but the knockout mice do not exhibit auditory or vestibular phenotypes [119]. Zebrafish *odf3l2a* is expressed in both inner ear and lateral line hair cells (Figure 1C) [55,122] whereas *odf3b* is specifically expressed in ciliated cells of the olfactory epithelia and pronephros [123]. Zebrafish have a second ortholog (*odf3l2b*) whose expression is restricted to the testis [124]. Thus, vertebrate hair cells may utilize different *ODF3* orthologs – *ODF3B* in mammals and *odf3l2a* in fish.

Saxo2 expression is enriched in mouse cochlear and vestibular hair cells [48,84,120,121] as well as the inner ear and lateral line hair cells of zebrafish (Figure 1D) [55,122]. Enriched expression in the olfactory epithelia is also shared between mice and fish [105]. However, unlike *Odf3l2*, there are no published loss-of-function animal models for *Saxo2*. Human *SAXO2* (a.k.a. *FAM154B*) and *ODF3L2* were reported in SHIELD as mapping to deafness loci *DFNA30* and *DFNB72*, respectively [27]. *DFNA30* is an autosomal dominant form of nonsyndromic hearing loss for which the causative gene remains unknown [85]. However, neither *SAXO2* or *ODF3L2* reside within any known deafness loci based on our analysis of the genetic markers used to map these and other nearby loci (Table 1). Although it is still possible that ODF3L2 and SAXO2 contribute to auditory and vestibular function, we propose they should be excluded as candidates for known deafness loci.

4.6. Benefits and limitations of this study.

In contrast to the short primary cilium of most cell types, sensory hair cells, in particular vestibular hair cells of the semicircular canals, possess very long kinocilia. This study takes advantage of the long kinocilium in the cristae of larval zebrafish and the ability to image tagged protein localization in live animals to understand more about the sub-cellular and sub-cilial localization of these proteins. Benefits of live imaging of fluorescently tagged proteins are i) avoiding morphological distortions caused by fixation and processing, and ii) inconsistent antibody staining. Limitations include the possibility of altered protein localization patterns caused by the fluorescent protein tag or from use of a heterologous promoter to drive overexpression. However, the fact that all three proteins

tested here display unique kinocilial and cytoplasmic distributions patterns suggest that these tagged proteins reflect their endogenous distribution patterns. An unexpected result from this study is Odf3l2a-GFP localization to the nucleus. Immunostaining of the endogenous protein is necessary to confirm this finding. If true, it presents the fascinating possibility of a communication channel between the kinocilia and the nucleus. Overexpression can also cause spurious phenotypes that may not be directly related to protein function. For example, the bulbed and truncated kinocilia observed in the "severe" Saxo2-mKate2 transgenic line may be an overexpression artifact caused by overloading the IFT machinery with excess Saxo2. However, the curved kinocilia we observe is consistent with previously reported function of MAP6-family proteins.

5. Conclusion

Here, we report hair cell-enriched expression of zebrafish *ankef1a*, *odf3l2a*, and *saxo2,* and show that tagged versions of these protein exhibit distinct distribution patterns within the kinocilium. Together, our results suggest that the hair cell kinocilium is regionalized along its proximal-distal axis.

Supplementary Materials: Figures S1-4, Tables S1-4, Video S1.

Author Contributions: Conceptualization, T.E.; formal analysis, T.E.; investigation, T.E., W.P.B., K.W., and A.V.; data curation, T.E.; writing—original draft preparation, T.E.; writing—review and editing, T.E., W.P.B., K.W., and A.V.; visualization, T.E. and A.V.; supervision, T.E.; project administration, T.E.; funding acquisition, T.E. All authors have read and agreed to the published version of the manuscript.

Funding: This work was supported by funding awarded to T.E. by the Collins Medical Trust, East Carolina University's Division of Research, Economic Development and Engagement (REDE), and The Natural Science and Engineering Research Council (NSERC) of Canada Discovery Grant RGPIN-2021-0316.

Institutional Review Board Statement: All procedures involving animals were performed in accordance with animal use protocols approved at Oregon Health & Science University (2065), East Carolina University (D352), and the University of New Brunswick (22007).

Data Availability Statement: Data and code will be provided by reasonable request from a qualified researcher.

Acknowledgments: This work as conducted at three institutions (OHSU, ECU, and UNB), intermittently over approximately eight years. A special thank you to Teresa Nicolson, in whose lab at OHSU this work was initiated. Thank you also to Amy Carlos and Robert Searles of the OHSU Massively Parallel Sequencing Shared Resource for performing the RNA sequencing experiments. Many thanks to the support staff in the Nicolson lab at OHSU and to the many students who have contributed to animal care at ECU and UNB. Thank you to Christine Erickson for making the hair cell diagrams.

Conflicts of Interest: The authors declare no conflict of interest.

589 ## 6. References

590 1. Bezares-Calderón, L.A.; Berger, J.; Jékely, G. Diversity of Cilia-Based
591 Mechanosensory Systems and Their Functions in Marine Animal Behaviour. *Philos*
592 *Trans R Soc Lond B Biol Sci* **2020**, *375*, 20190376, doi:10.1098/rstb.2019.0376.

593 2. Sharkova, M.; Chow, E.; Erickson, T.; Hocking, J.C. The Morphological and
594 Functional Diversity of Apical Microvilli. *J Anat* **2022**, doi:10.1111/joa.13781.

595 3. Jones, C.; Roper, V.C.; Foucher, I.; Qian, D.; Banizs, B.; Petit, C.; Yoder, B.K.;
596 Chen, P. Ciliary Proteins Link Basal Body Polarization to Planar Cell Polarity
597 Regulation. *Nat Genet* **2008**, *40*, 69–77, doi:10.1038/ng.2007.54.

598 4. Moon, K.-H.; Ma, J.-H.; Min, H.; Koo, H.; Kim, H.; Ko, H.W.; Bok, J.
599 Dysregulation of Sonic Hedgehog Signaling Causes Hearing Loss in Ciliopathy
600 Mouse Models. *Elife* **2020**, *9*, 1–63, doi:10.7554/eLife.56551.

601 5. Shi, H.; Wang, H.; Zhang, C.; Lu, Y.; Yao, J.; Chen, Z.; Xing, G.; Wei, Q.; Cao, X.
602 Mutations in OSBPL2 Cause Hearing Loss Associated with Primary Cilia Defects
603 via Sonic Hedgehog Signaling. *JCI Insight* **2022**, *7*, doi:10.1172/jci.insight.149626.

604 6. Baird, R.A. Comparative Transduction Mechanisms of Hair Cells in the Bullfrog
605 Utriculus. II. Sensitivity and Response Dynamics to Hair Bundle Displacement. *J*
606 *Neurophysiol* **1994**, *71*, 685–705, doi:10.1152/jn.1994.71.2.685.

607 7. Spoon, C.; Grant, W. Biomechanics of Hair Cell Kinocilia: Experimental
608 Measurement of Kinocilium Shaft Stiffness and Base Rotational Stiffness with
609 Euler–Bernoulli and Timoshenko Beam Analysis. *Journal of Experimental Biology*
610 **2011**, *214*, 862–870, doi:10.1242/jeb.051151.

611 8. Kindt, K.S.; Finch, G.; Nicolson, T. Kinocilia Mediate Mechanosensitivity in
612 Developing Zebrafish Hair Cells. *Dev Cell* **2012**, *23*, 329–341,
613 doi:10.1016/j.devcel.2012.05.022.

614 9. Stooke-Vaughan, G.A.; Huang, P.; Hammond, K.L.; Schier, A.F.; Whitfield, T.T.
615 The Role of Hair Cells, Cilia and Ciliary Motility in Otolith Formation in the
616 Zebrafish Otic Vesicle. *Development* **2012**, *139*, 1777–1787,
617 doi:10.1242/dev.079947.

618 10. Sobkowicz, H.M.; Slapnick, S.M.; August, B.K. The Kinocilium of Auditory Hair
619 Cells and Evidence for Its Morphogenetic Role during the Regeneration of
620 Stereocilia and Cuticular Plates. *J Neurocytol* **1995**, *24*, 633–653,
621 doi:10.1007/BF01179815.

622 11. Flock, A.; Duvall, A.J. The Ultrastructure of the Kinocilium of the Sensory Cells in
623 the Inner Ear and Lateral Line Organs. *Journal of Cell Biology* **1965**, *25*, 1–8,
624 doi:10.1083/jcb.25.1.1.

625 12. Kikuchi, T.; Takasaka, T.; Tonosaki, A.; Watanabe, H. Fine Structure of Guinea Pig
626 Vestibular Kinocilium. *Acta Otolaryngol* **1989**, *108*, 26–30,
627 doi:10.3109/00016488909107388.

628 13. Burton, P.R. Ultrastructural Studies of Microtubules and Microtubule Organizing
629 Centers of the Vertebrate Olfactory Neuron. *Microsc Res Tech* **1992**, *23*, 142–156,
630 doi:10.1002/jemt.1070230205.

631 14. Rüsch, A.; Thurm, U. Passive and Active Deflections of Ampullary Kinocilia
632 Correlated with Changes in Transepithelial Voltage. *ORL* **1986**, *48*, 76–80,
633 doi:10.1159/000275849.

634 15. Rüsch, A.; Thurm, U. Spontaneous and Electrically Induced Movements of
635 Ampullary Kinocilia and Stereovilli. *Hear Res* **1990**, *48*, 247–263,
636 doi:10.1016/0378-5955(90)90065-W.

637 16. Alstrom, C.H.; Hallgren, B.; Nilsson, L.; Asander, H. Retinal Degeneration
638 Combined with Obesity, Diabetes Mellitus and Neurogenous Deafness: A Specific
639 Syndrome (Not Hitherto Described) Distinct from the Laurence-Moon-Bardet-Biedl
640 Syndrome: A Clinical, Endocrinological and Genetic Examination Based on a Large
641 Pedigree. *Acta Psychiatr Neurol Scand Suppl* **1959**, *129*, 1–35.

642 17. Ross, A.J.; May-Simera, H.; Eichers, E.R.; Kai, M.; Hill, J.; Jagger, D.J.; Leitch,
643 C.C.; Chapple, J.P.; Munro, P.M.; Fisher, S.; et al. Disruption of Bardet-Biedl
644 Syndrome Ciliary Proteins Perturbs Planar Cell Polarity in Vertebrates. *Nature*
645 *Genetics 2005 37:10* **2005**, *37*, 1135–1140, doi:10.1038/ng1644.

646 18. Jagger, D.; Collin, G.; Kelly, J.; Towers, E.; Nevill, G.; Longo-Guess, C.; Benson,
647 J.; Halsey, K.; Dolan, D.; Marshall, J.; et al. Alström Syndrome Protein ALMS1
648 Localizes to Basal Bodies of Cochlear Hair Cells and Regulates Cilium-Dependent
649 Planar Cell Polarity. *Hum Mol Genet* **2011**, *20*, 466–481, doi:10.1093/hmg/ddq493.

650 19. Modamio-Høybjør, S.; Mencía, Á.; Goodyear, R.; del Castillo, I.; Richardson, G.;
651 Moreno, F.; Moreno-Pelayo, M.Á. A Mutation in CCDC50, a Gene Encoding an
652 Effector of Epidermal Growth Factor-Mediated Cell Signaling, Causes Progressive
653 Hearing Loss. *Am J Hum Genet* **2007**, *80*, 1076–1089, doi:10.1086/518311.

654 20. Cui, L.; Zheng, J.; Zhao, Q.; Chen, J.-R.; Liu, H.; Peng, G.; Wu, Y.; Chen, C.; He,
655 Q.; Shi, H.; et al. Mutations of MAP1B Encoding a Microtubule-Associated
656 Phosphoprotein Cause Sensorineural Hearing Loss. *JCI Insight* **2020**, *5*,
657 doi:10.1172/jci.insight.136046.

658 21. Grati, M.; Chakchouk, I.; Ma, Q.; Bensaid, M.; Desmidt, A.; Turki, N.; Yan, D.;
659 Baanannou, A.; Mittal, R.; Driss, N.; et al. A Missense Mutation in DCDC2 Causes
660 Human Recessive Deafness DFNB66, Likely by Interfering with Sensory Hair Cell
661 and Supporting Cell Cilia Length Regulation. *Hum Mol Genet* **2015**, *24*, 2482–2491,
662 doi:10.1093/hmg/ddv009.

663 22. Bork, J.M.; Peters, L.M.; Riazuddin, S.; Ahmed, Z.M.; Li, X.C.; Griffith, A.J.;
664 Wilcox, E.R.; Friedman, T.B.; Morell, R.J.; Griffith, A.J.; et al. Usher Syndrome 1D
665 and Nonsyndromic Autosomal Recessive Deafness DFNB12 Are Caused by Allelic
666 Mutations of the Novel Cadherin-like Gene CDH23. *Am J Hum Genet* **2001**, *68*, 26–
667 37, doi:10.1086/316954.

668 23. Ahmed, Z.M. PCDH15 Is Expressed in the Neurosensory Epithelium of the Eye and
669 Ear and Mutant Alleles Are Responsible for Both USH1F and DFNB23. *Hum Mol*
670 *Genet* **2003**, *12*, 3215–3223, doi:10.1093/hmg/ddg358.

671 24. Pickett, S.B.; Raible, D.W. Water Waves to Sound Waves: Using Zebrafish to
672 Explore Hair Cell Biology. *Journal of the Association for Research in*
673 *Otolaryngology* **2019**, *20*, 1–19, doi:10.1007/s10162-018-00711-1.

674 25. Gunn, R.K.; Keenan, M.-E.; Brown, R.E. Analysis of Sensory, Motor and Cognitive
675 Functions of the Coloboma (C3Sn.Cg-Cm/J) Mutant Mouse. *Genes Brain Behav*
676 **2011**, *10*, 579–588, doi:10.1111/j.1601-183X.2011.00697.x.

677 26. Kiernan, A.E.; Ahituv, N.; Fuchs, H.; Balling, R.; Avraham, K.B.; Steel, K.P.; Hrabé
678 de Angelis, M. The Notch Ligand Jagged1 Is Required for Inner Ear Sensory
679 Development. *Proc Natl Acad Sci U S A* **2001**, *98*, 3873–3878,
680 doi:10.1073/pnas.071496998.

681 27. Shen, J.; Scheffer, D.I.; Kwan, K.Y.; Corey, D.P. SHIELD: An Integrative Gene
682 Expression Database for Inner Ear Research. *Database (Oxford)* **2015**, *2015*,
683 bav071, doi:10.1093/database/bav071.

684 28. Westerfield, M. *The Zebrafish Book. A Guide for the Laboratory Use of Zebrafish*
685 *(Danio Rerio).*; 4th ed.; University of Oregon: Eugene OR, 2000;

686 29. Ohta, S.; Ji, Y.R.; Martin, D.; Wu, D.K. Emx2 Regulates Hair Cell Rearrangement
687 but Not Positional Identity within Neuromasts. *Elife* **2020**, *9*, 1–69,
688 doi:10.7554/eLife.60432.

689 30. Erickson, T.; Nicolson, T. Identification of Sensory Hair-Cell Transcripts by
690 Thiouracil-Tagging in Zebrafish. *BMC Genomics* **2015**, *16*, 842,
691 doi:10.1186/s12864-015-2072-5.

692 31. Kwan, K.M.; Fujimoto, E.; Grabher, C.; Mangum, B.D.; Hardy, M.E.; Campbell,
693 D.S.; Parant, J.M.; Yost, H.J.; Kanki, J.P.; Chien, C.-B. The Tol2kit: A Multisite
694 Gateway-Based Construction Kit for Tol2 Transposon Transgenesis Constructs.
695 *Developmental Dynamics* **2007**, *236*, 3088–3099, doi:10.1002/dvdy.21343.

696 32. Afgan, E.; Baker, D.; van den Beek, M.; Blankenberg, D.; Bouvier, D.; Čech, M.;
697 Chilton, J.; Clements, D.; Coraor, N.; Eberhard, C.; et al. The Galaxy Platform for
698 Accessible, Reproducible and Collaborative Biomedical Analyses: 2016 Update.
699 *Nucleic Acids Res* **2016**, *44*, W3–W10, doi:10.1093/nar/gkw343.

700 33. Thomas, P.D.; Ebert, D.; Muruganujan, A.; Mushayahama, T.; Albou, L.; Mi, H.
701 <scp>PANTHER</Scp> : Making Genome-scale Phylogenetics Accessible to All.
702 *Protein Science* **2022**, *31*, 8–22, doi:10.1002/pro.4218.

703 34. Mi, H.; Muruganujan, A.; Huang, X.; Ebert, D.; Mills, C.; Guo, X.; Thomas, P.D.
704 Protocol Update for Large-Scale Genome and Gene Function Analysis with the
705 PANTHER Classification System (v.14.0). *Nature Protocols 2019 14:3* **2019**, *14*,
706 703–721, doi:10.1038/s41596-019-0128-8.

707 35. van Camp, G.; Smith, R.J.H. Hereditary Hearing Loss Homepage Available online:
708 https://hereditaryhearingloss.org (accessed on 29 December 2022).

709 36. Cunningham, F.; Allen, J.E.; Allen, J.; Alvarez-Jarreta, J.; Amode, M.R.; Armean,
710 I.M.; Austine-Orimoloye, O.; Azov, A.G.; Barnes, I.; Bennett, R.; et al. Ensembl
711 2022. *Nucleic Acids Res* **2022**, *50*, D988–D995, doi:10.1093/NAR/GKAB1049.

712 37. Schindelin, J.; Arganda-Carreras, I.; Frise, E.; Kaynig, V.; Longair, M.; Pietzsch,
713 T.; Preibisch, S.; Rueden, C.; Saalfeld, S.; Schmid, B.; et al. Fiji: An Open-Source
714 Platform for Biological-Image Analysis. *Nat Methods* **2012**, *9*, 676–682,
715 doi:10.1038/nmeth.2019.

716 38. Schneider, C.A.; Rasband, W.S.; Eliceiri, K.W. NIH Image to ImageJ: 25 Years of
717 Image Analysis. *Nat Methods* **2012**, *9*, 671–675, doi:10.1038/nmeth.2089.

718 39. Arshadi, C.; Günther, U.; Eddison, M.; Harrington, K.I.S.; Ferreira, T.A. SNT: A
719 Unifying Toolbox for Quantification of Neuronal Anatomy. *Nature Methods 2021*
720 *18:4* **2021**, *18*, 374–377, doi:10.1038/s41592-021-01105-7.

721 40. RStudio Team RStudio: Integrated Development Environment for R 2022.

722 41. R Core Team R: A Language and Environment for Statistical Computing 2022.

723 42. Wickham, H. Ggplot2. *Wiley Interdiscip Rev Comput Stat* **2011**, *3*, 180–185,
724 doi:10.1002/wics.147.

725 43. Miller, M.R.; Robinson, K.J.; Cleary, M.D.; Doe, C.Q. TU-Tagging: Cell Type-
726 Specific RNA Isolation from Intact Complex Tissues. *Nat Methods* **2009**, *6*, 439–
727 441, doi:10.1038/nmeth.1329.

728 44. Daniel, J.G.; Panizzi, J.R. Spatiotemporal Expression Profile of Embryonic and
729 Adult Ankyrin Repeat and EF-Hand Domain Containing Protein 1-Encoding Genes
730 Ankef1a and Ankef1b in Zebrafish. *Gene Expression Patterns* **2019**, *34*, 119069,
731 doi:10.1016/j.gep.2019.119069.

732 45. Scott, E.K.; Mason, L.; Arrenberg, A.B.; Ziv, L.; Gosse, N.J.; Xiao, T.; Chi, N.C.;
733 Asakawa, K.; Kawakami, K.; Baier, H. Targeting Neural Circuitry in Zebrafish
734 Using GAL4 Enhancer Trapping. *Nature Methods 2007 4:4* **2007**, *4*, 323–326,
735 doi:10.1038/nmeth1033.

736 46. Chung, H.A.; Yamamoto, T.S.; Ueno, N. ANR5, an FGF Target Gene Product,
737 Regulates Gastrulation in Xenopus. *Current Biology* **2007**, *17*, 932–939,
738 doi:10.1016/j.cub.2007.04.034.

739 47. di Domenico, F. The Role of Ankef1 in Male Fertility, Icahn School of Medicine at
740 Mount Sinai: New York, 2021.

741 48. Jan, T.A.; Eltawil, Y.; Ling, A.H.; Chen, L.; Ellwanger, D.C.; Heller, S.; Cheng,
742 A.G. Spatiotemporal Dynamics of Inner Ear Sensory and Non-Sensory Cells
743 Revealed by Single-Cell Transcriptomics. *Cell Rep* **2021**, *36*, 109358,
744 doi:10.1016/j.celrep.2021.109358.

745 49. Hoh, R.A.; Stowe, T.R.; Turk, E.; Stearns, T. Transcriptional Program of Ciliated
746 Epithelial Cells Reveals New Cilium and Centrosome Components and Links to
747 Human Disease. *PLoS One* **2012**, *7*, e52166, doi:10.1371/journal.pone.0052166.

50. Baker, M.A.; Hetherington, L.; Reeves, G.M.; Aitken, R.J. The Mouse Sperm Proteome Characterizedvia IPG Strip Prefractionation and LC-MS/MS Identification. *Proteomics* **2008**, *8*, 1720–1730, doi:10.1002/pmic.200701020.

51. Baker, M.A.; Hetherington, L.; Reeves, G.; Müller, J.; Aitken, R.J. The Rat Sperm Proteome Characterized ***via*** IPG Strip Prefractionation and LC-MS/MS Identification. *Proteomics* **2008**, *8*, 2312–2321, doi:10.1002/pmic.200700876.

52. Blackburn, K.; Bustamante-Marin, X.; Yin, W.; Goshe, M.B.; Ostrowski, L.E. Quantitative Proteomic Analysis of Human Airway Cilia Identifies Previously Uncharacterized Proteins of High Abundance. *J Proteome Res* **2017**, *16*, 1579–1592, doi:10.1021/acs.jproteome.6b00972.

53. Elkon, R.; Milon, B.; Morrison, L.; Shah, M.; Vijayakumar, S.; Racherla, M.; Leitch, C.C.; Silipino, L.; Hadi, S.; Weiss-Gayet, M.; et al. RFX Transcription Factors Are Essential for Hearing in Mice. *Nat Commun* **2015**, *6*, 8549, doi:10.1038/ncomms9549.

54. Lush, M.E.; Diaz, D.C.; Koenecke, N.; Baek, S.; Boldt, H.; St Peter, M.K.; Gaitan-Escudero, T.; Romero-Carvajal, A.; Busch-Nentwich, E.M.; Perera, A.G.; et al. ScRNA-Seq Reveals Distinct Stem Cell Populations That Drive Hair Cell Regeneration after Loss of Fgf and Notch Signaling. *Elife* **2019**, *8*, doi:10.7554/eLife.44431.

55. Barta, C.L.; Liu, H.; Chen, L.; Giffen, K.P.; Li, Y.; Kramer, K.L.; Beisel, K.W.; He, D.Z. RNA-Seq Transcriptomic Analysis of Adult Zebrafish Inner Ear Hair Cells. *Sci Data* **2018**, *5*, 180005, doi:10.1038/sdata.2018.5.

56. Hess, E.J.; Collins, K.A.; Copeland, N.G.; Jenkins, N.A.; Wilson, M.C. Deletion Map of the Coloboma (Cm) Locus on Mouse Chromosome 2. *Genomics* **1994**, *21*, 257–261, doi:10.1006/geno.1994.1254.

57. Blake, J.A.; Baldarelli, R.; Kadin, J.A.; Richardson, J.E.; Smith, C.L.; Bult, C.J.; Anagnostopoulos, A. v; Beal, J.S.; Bello, S.M.; Blodgett, O.; et al. Mouse Genome Database (MGD): Knowledgebase for Mouse–Human Comparative Biology. *Nucleic Acids Res* **2021**, *49*, D981–D987, doi:10.1093/nar/gkaa1083.

58. Hess, E.; Jinnah, H.; Kozak, C.; Wilson, M. Spontaneous Locomotor Hyperactivity in a Mouse Mutant with a Deletion Including the Snap Gene on Chromosome 2. *The Journal of Neuroscience* **1992**, *12*, 2865–2874, doi:10.1523/JNEUROSCI.12-07-02865.1992.

59. Egydio de Carvalho, C.; Tanaka, H.; Iguchi, N.; Ventelä, S.; Nojima, H.; Nishimune, Y. Molecular Cloning and Characterization of a Complementary DNA Encoding Sperm Tail Protein SHIPPO 11. *Biol Reprod* **2002**, *66*, 785–795, doi:10.1095/biolreprod66.3.785.

60. Dorus, S.; Busby, S.A.; Gerike, U.; Shabanowitz, J.; Hunt, D.F.; Karr, T.L. Genomic and Functional Evolution of the Drosophila Melanogaster Sperm Proteome. *Nat Genet* **2006**, *38*, 1440–1445, doi:10.1038/ng1915.

61. Konno, A.; Padma, P.; Ushimaru, Y.; Inaba, K. Multidimensional Analysis of Uncharacterized Sperm Proteins in *Ciona Intestinalis* : EST-Based Analysis and

790 Functional Immunoscreening of Testis-Expressed Genes. *Zoolog Sci* **2010**, *27*, 204–
791 215, doi:10.2108/zsj.27.204.

792 62. Konno, A.; Shiba, K.; Cai, C.; Inaba, K. Branchial Cilia and Sperm Flagella Recruit
793 Distinct Axonemal Components. *PLoS One* **2015**, *10*, e0126005,
794 doi:10.1371/journal.pone.0126005.

795 63. White-Cooper, H. Studying How Flies Make Sperm—Investigating Gene Function
796 in Drosophila Testes. *Mol Cell Endocrinol* **2009**, *306*, 66–74,
797 doi:10.1016/j.mce.2008.11.026.

798 64. Bastin, B.R. Evolution of Tektin and ODF3 Family Genes and the Role of Gene
799 Duplication in the Specialization of Motile Ciliary Structures in the Polychaete
800 Platynereis Dumerilii, Iowa State University, 2018.

801 65. Lauwaet, T.; Smith, A.J.; Reiner, D.S.; Romijn, E.P.; Wong, C.C.L.; Davids, B.J.;
802 Shah, S.A.; Yates, J.R.; Gillin, F.D. Mining the Giardia Genome and Proteome for
803 Conserved and Unique Basal Body Proteins. *Int J Parasitol* **2011**, *41*, 1079–1092,
804 doi:10.1016/j.ijpara.2011.06.001.

805 66. Fong, K.; Leung, J.W.; Li, Y.; Wang, W.; Feng, L.; Ma, W.; Liu, D.; Songyang, Z.;
806 Chen, J. MTR120/KIAA1383, a Novel Microtubule-Associated Protein, Promotes
807 Microtubule Stability and Ensures Cytokinesis. *J Cell Sci* **2013**, *126*, 825–837,
808 doi:10.1242/jcs.116137.

809 67. Bowl, M.R.; Simon, M.M.; Ingham, N.J.; Greenaway, S.; Santos, L.; Cater, H.;
810 Taylor, S.; Mason, J.; Kurbatova, N.; Pearson, S.; et al. A Large Scale Hearing Loss
811 Screen Reveals an Extensive Unexplored Genetic Landscape for Auditory
812 Dysfunction. *Nat Commun* **2017**, *8*, 886, doi:10.1038/s41467-017-00595-4.

813 68. Rehman, A.U.; Gul, K.; Morell, R.J.; Lee, K.; Ahmed, Z.M.; Riazuddin, S.; Ali,
814 R.A.; Shahzad, M.; Jaleel, A.; Andrade, P.B.; et al. Mutations of GIPC3 Cause
815 Nonsyndromic Hearing Loss DFNB72 but Not DFNB81 That Also Maps to
816 Chromosome 19p. *Hum Genet* **2011**, *130*, 759–765, doi:10.1007/s00439-011-1018-
817 5.

818 69. Charizopoulou, N.; Lelli, A.; Schraders, M.; Ray, K.; Hildebrand, M.S.; Ramesh,
819 A.; Srisailapathy, C.R.S.; Oostrik, J.; Admiraal, R.J.C.; Neely, H.R.; et al. Gipc3
820 Mutations Associated with Audiogenic Seizures and Sensorineural Hearing Loss in
821 Mouse and Human. *Nat Commun* **2011**, *2*, 201, doi:10.1038/ncomms1200.

822 70. Santos-Cortez, R.L.P.; Faridi, R.; Rehman, A.U.; Lee, K.; Ansar, M.; Wang, X.;
823 Morell, R.J.; Isaacson, R.; Belyantseva, I.A.; Dai, H.; et al. Autosomal-Recessive
824 Hearing Impairment Due to Rare Missense Variants within S1PR2. *Am J Hum Genet*
825 **2016**, *98*, 331–338, doi:10.1016/j.ajhg.2015.12.004.

826 71. Jenkinson, E.M.; Rehman, A.U.; Walsh, T.; Clayton-Smith, J.; Lee, K.; Morell, R.J.;
827 Drummond, M.C.; Khan, S.N.; Naeem, M.A.; Rauf, B.; et al. Perrault Syndrome Is
828 Caused by Recessive Mutations in CLPP, Encoding a Mitochondrial ATP-
829 Dependent Chambered Protease. *Am J Hum Genet* **2013**, *92*, 605–613,
830 doi:10.1016/j.ajhg.2013.02.013.

72. Bönsch, D.; Schmidt, C.M.; Scheer, P.; Bohlender, J.; Neumann, C.; am Zehnhoff-Dinnesen, A.; Deufel, T. Ein Neuer Genort Für Eine Autosomal Dominante, Nichtsyndromale Hörstörung (DFNA57) Kartiert Auf Chromosom 19p13.2 Und Überlappt Mit DFNB15. *HNO* **2008**, *56*, 177–182, doi:10.1007/s00106-007-1633-6.

73. Ain, Q.; Nazli, S.; Riazuddin, S.; Jaleel, A.; Riazuddin, S.A.; Zafar, A.U.; Khan, S.N.; Husnain, T.; Griffith, A.J.; Ahmed, Z.M.; et al. The Autosomal Recessive Nonsyndromic Deafness Locus DFNB72 Is Located on Chromosome 19p13.3. *Hum Genet* **2007**, *122*, 445–450, doi:10.1007/s00439-007-0418-z.

74. Cuveillier, C.; Boulan, B.; Ravanello, C.; Denarier, E.; Deloulme, J.-C.; Gory-Fauré, S.; Delphin, C.; Bosc, C.; Arnal, I.; Andrieux, A. Beyond Neuronal Microtubule Stabilization: MAP6 and CRMPS, Two Converging Stories. *Front Mol Neurosci* **2021**, *14*, 82, doi:10.3389/fnmol.2021.665693.

75. Dacheux, D.; Landrein, N.; Thonnus, M.; Gilbert, G.; Sahin, A.; Wodrich, H.; Robinson, D.R.; Bonhivers, M. A MAP6-Related Protein Is Present in Protozoa and Is Involved in Flagellum Motility. *PLoS One* **2012**, *7*, e31344, doi:10.1371/journal.pone.0031344.

76. Dacheux, D.; Roger, B.; Bosc, C.; Landrein, N.; Roche, E.; Chansel, L.; Trian, T.; Andrieux, A.; Papaxanthos-Roche, A.; Marthan, R.; et al. Human FAM154A (SAXO1) Is a Microtubule-Stabilizing Protein Specific to Cilia and Related Structures. *J Cell Sci* **2015**, *128*, 1294–1307, doi:10.1242/jcs.155143.

77. Onyeneho, I.A. Microtubule Stability Mediated by New Mammalian STOP Family Members, Stanford University, 2014.

78. Kim, K.; Gibboney, S.; Razy-Krajka, F.; Lowe, E.K.; Wang, W.; Stolfi, A. Regulation of Neurogenesis by FGF Signaling and Neurogenin in the Invertebrate Chordate Ciona. *Front Cell Dev Biol* **2020**, *8*, 477, doi:10.3389/fcell.2020.00477.

79. Leung, M.R.; Roelofs, M.C.; Chiozzi, R.Z.; Hevler, J.F.; Heck, A.J.R.; Zeev-Ben-Mordehai, T. Unraveling the Intricate Microtubule Inner Protein Networks That Reinforce Mammalian Sperm Flagella. *bioRxiv* **2022**, 2022.09.29.510157, doi:10.1101/2022.09.29.510157.

80. Gui, M.; Wang, X.; Dutcher, S.K.; Brown, A.; Zhang, R. Ciliary Central Apparatus Structure Reveals Mechanisms of Microtubule Patterning. *Nat Struct Mol Biol* **2022**, *29*, 483–492, doi:10.1038/s41594-022-00770-2.

81. Gui, M.; Croft, J.T.; Zabeo, D.; Acharya, V.; Kollman, J.M.; Burgoyne, T.; Höög, J.L.; Brown, A. SPACA9 Is a Lumenal Protein of Human Ciliary Singlet and Doublet Microtubules. *Proc Natl Acad Sci U S A* **2022**, *119*, e2207605119, doi:10.1073/pnas.2207605119.

82. Ichikawa, M.; Bui, K.H. Microtubule Inner Proteins: A Meshwork of Luminal Proteins Stabilizing the Doublet Microtubule. *BioEssays* **2018**, *40*, 1700209, doi:10.1002/bies.201700209.

83. Cuveillier, C.; Delaroche, J.; Seggio, M.; Gory-Fauré, S.; Bosc, C.; Denarier, E.; Bacia, M.; Schoehn, G.; Mohrbach, H.; Kulić, I.; et al. MAP6 Is an Intraluminal

873 Protein That Induces Neuronal Microtubules to Coil. *Sci Adv* **2020**, *6*,
874 doi:10.1126/sciadv.aaz4344.

875 84. Wilkerson, B.A.; Zebroski, H.L.; Finkbeiner, C.R.; Chitsazan, A.D.; Beach, K.E.;
876 Sen, N.; Zhang, R.C.; Bermingham-McDonogh, O. Novel Cell Types and
877 Developmental Lineages Revealed by Single-Cell RNA-Seq Analysis of the Mouse
878 Crista Ampullaris. *Elife* **2021**, *10*, doi:10.7554/eLife.60108.

879 85. Mangino, M.; Flex, E.; Capon, F.; Sangiuolo, F.; Carraro, E.; Gualandi, F.; Mazzoli,
880 M.; Martini, A.; Novelli, G.; Dallapiccola, B. Mapping of a New Autosomal
881 Dominant Nonsyndromic Hearing Loss Locus (DFNA30) to Chromosome 15q25-
882 26. *European Journal of Human Genetics* **2001**, *9*, 667–671,
883 doi:10.1038/sj.ejhg.5200707.

884 86. Azaiez, H.; Decker, A.R.; Booth, K.T.; Simpson, A.C.; Shearer, A.E.; Huygen,
885 P.L.M.; Bu, F.; Hildebrand, M.S.; Ranum, P.T.; Shibata, S.B.; et al. HOMER2, a
886 Stereociliary Scaffolding Protein, Is Essential for Normal Hearing in Humans and
887 Mice. *PLoS Genet* **2015**, *11*, e1005137, doi:10.1371/journal.pgen.1005137.

888 87. Lu, X.; Wang, Q.; Gu, H.; Zhang, X.; Qi, Y.; Liu, Y. Whole Exome Sequencing
889 Identified a Second Pathogenic Variant in HOMER2 for Autosomal Dominant Non-
890 Syndromic Deafness. *Clin Genet* **2018**, *94*, 419–428, doi:10.1111/cge.13422.

891 88. Ahmad, J.; Khan, S.N.; Khan, S.Y.; Ramzan, K.; Riazuddin, S.; Ahmed, Z.M.;
892 Wilcox, E.R.; Friedman, T.B.; Riazuddin, S. DFNB48, a New Nonsyndromic
893 Recessive Deafness Locus, Maps to Chromosome 15q23-Q25.1. *Hum Genet* **2005**,
894 *116*, 407–412, doi:10.1007/s00439-004-1247-y.

895 89. Riazuddin, S.; Belyantseva, I.A.; Giese, A.P.J.; Lee, K.; Indzhykulian, A.A.;
896 Nandamuri, S.P.; Yousaf, R.; Sinha, G.P.; Lee, S.; Terrell, D.; et al. Alterations of
897 the CIB2 Calcium- and Integrin-Binding Protein Cause Usher Syndrome Type 1J
898 and Nonsyndromic Deafness DFNB48. *Nat Genet* **2012**, *44*, 1265–1271,
899 doi:10.1038/ng.2426.

900 90. Tomek, M.S.; Brown, M.R.; Mani, S.R.; Ramesh, A.; Srisailapathy, C.R.; Coucke,
901 P.; Zbar, R.I.; Bell, A.M.; McGuirt, W.T.; Fukushima, K.; et al. Localization of a
902 Gene for Otosclerosis to Chromosome 15q25-Q26. *Hum Mol Genet* **1998**, *7*, 285–
903 290, doi:10.1093/hmg/7.2.285.

904 91. Wang, S.; Hazelrigg, T. Implications for Bcd MRNA Localization from Spatial
905 Distribution of Exu Protein in Drosophila Oogenesis. *Nature* **1994**, *369*, 400–403,
906 doi:10.1038/369400a0.

907 92. Gerdes, H.-H.; Kaether, C. Green Fluorescent Protein: Applications in Cell Biology.
908 *FEBS Lett* **1996**, *389*, 44–47, doi:10.1016/0014-5793(96)00586-8.

909 93. Sheets, L.; He, X.J.; Olt, J.; Schreck, M.; Petralia, R.S.; Wang, Y.-X.; Zhang, Q.;
910 Beirl, A.; Nicolson, T.; Marcotti, W.; et al. Enlargement of Ribbons in Zebrafish
911 Hair Cells Increases Calcium Currents But Disrupts Afferent Spontaneous Activity
912 and Timing of Stimulus Onset. *The Journal of Neuroscience* **2017**, *37*, 6299–6313,
913 doi:10.1523/JNEUROSCI.2878-16.2017.

914 94. Maeda, R.; Pacentine, I. v; Erickson, T.; Nicolson, T. Functional Analysis of the
915 Transmembrane and Cytoplasmic Domains of Pcdh15a in Zebrafish Hair Cells. *J*
916 *Neurosci* **2017**, *37*, 3231–3245, doi:10.1523/JNEUROSCI.2216-16.2017.

917 95. Erickson, T.; Pacentine, I. v.; Venuto, A.; Clemens, R.; Nicolson, T. The Lhfpl5
918 Ohnologs Lhfpl5a and Lhfpl5b Are Required for Mechanotransduction in Distinct
919 Populations of Sensory Hair Cells in Zebrafish. *Front Mol Neurosci* **2020**, *12*, 320,
920 doi:10.3389/fnmol.2019.00320.

921 96. Erickson, T.; Morgan, C.P.; Olt, J.; Hardy, K.; Busch-Nentwich, E.; Maeda, R.;
922 Clemens, R.; Krey, J.F.; Nechiporuk, A.; Barr-Gillespie, P.G.; et al. Integration of
923 Tmc1/2 into the Mechanotransduction Complex in Zebrafish Hair Cells Is Regulated
924 by Transmembrane O-Methyltransferase (Tomt). *Elife* **2017**, *6*,
925 doi:10.7554/eLife.28474.

926 97. Pacentine, I. v.; Nicolson, T. Subunits of the Mechano-Electrical Transduction
927 Channel, Tmc1/2b, Require Tmie to Localize in Zebrafish Sensory Hair Cells. *PLoS*
928 *Genet* **2019**, *15*, e1007635, doi:10.1371/journal.pgen.1007635.

929 98. Gopal, S.R.; Chen, D.H.-C.; Chou, S.-W.; Zang, J.; Neuhauss, S.C.F.; Stepanyan,
930 R.; McDermott, B.M.; Alagramam, K.N. Zebrafish Models for the Mechanosensory
931 Hair Cell Dysfunction in Usher Syndrome 3 Reveal That Clarin-1 Is an Essential
932 Hair Bundle Protein. *Journal of Neuroscience* **2015**, *35*, 10188–10201,
933 doi:10.1523/JNEUROSCI.1096-15.2015.

934 99. Smith, E.T.; Pacentine, I.; Shipman, A.; Hill, M.; Nicolson, T. Disruption of
935 Tmc1/2a/2b Genes in Zebrafish Reveals Subunit Requirements in Subtypes of Inner
936 Ear Hair Cells. *J Neurosci* **2020**, *40*, 4457–4468, doi:10.1523/JNEUROSCI.0163-
937 20.2020.

938 100. Chen, Z.; Chou, S.-W.; McDermott, B.M. Ribeye Protein Is Intrinsically Dynamic
939 but Is Stabilized in the Context of the Ribbon Synapse. *J Physiol* **2018**, *596*, 409–
940 421, doi:10.1113/JP271215.

941 101. Hwang, P.; Chou, S.-W.; Chen, Z.; McDermott, B.M. The Stereociliary Paracrystal
942 Is a Dynamic Cytoskeletal Scaffold In Vivo. *Cell Rep* **2015**, *13*, 1287–1294,
943 doi:10.1016/j.celrep.2015.10.003.

944 102. Sheets, L.; Hagen, M.W.; Nicolson, T. Characterization of Ribeye Subunits in
945 Zebrafish Hair Cells Reveals That Exogenous Ribeye B-Domain and CtBP1
946 Localize to the Basal Ends of Synaptic Ribbons. *PLoS One* **2014**, *9*, e107256,
947 doi:10.1371/journal.pone.0107256.

948 103. Choksi, S.P.; Babu, D.; Lau, D.; Yu, X.; Roy, S. Systematic Discovery of Novel
949 Ciliary Genes through Functional Genomics in the Zebrafish. *Development* **2014**,
950 *141*, 3410–3419, doi:10.1242/dev.108209.

951 104. Walentek, P.; Quigley, I.K.; Sun, D.I.; Sajjan, U.K.; Kintner, C.; Harland, R.M.
952 Ciliary Transcription Factors and MiRNAs Precisely Regulate Cp110 Levels
953 Required for Ciliary Adhesions and Ciliogenesis. *Elife* **2016**, *5*,
954 doi:10.7554/eLife.17557.

955 105. Stauber, M.; Weidemann, M.; Dittrich-Breiholz, O.; Lobschat, K.; Alten, L.; Mai,
956 M.; Beckers, A.; Kracht, M.; Gossler, A. Identification of FOXJ1 Effectors during
957 Ciliogenesis in the Foetal Respiratory Epithelium and Embryonic Left-Right
958 Organiser of the Mouse. *Dev Biol* **2017**, *423*, 170–188,
959 doi:10.1016/j.ydbio.2016.11.019.

960 106. Alsolami, M.; Kuhns, S.; Alsulami, M.; Blacque, O.E. ERICH3 in Primary Cilia
961 Regulates Cilium Formation and the Localisations of Ciliary Transport and Sonic
962 Hedgehog Signaling Proteins. *Scientific Reports 2019 9:1* **2019**, *9*, 1–13,
963 doi:10.1038/s41598-019-52830-1.

964 107. Imtiaz, A.; Belyantseva, I.A.; Beirl, A.J.; Fenollar-Ferrer, C.; Bashir, R.; Bukhari,
965 I.; Bouzid, A.; Shaukat, U.; Azaiez, H.; Booth, K.T.; et al. CDC14A Phosphatase Is
966 Essential for Hearing and Male Fertility in Mouse and Human. *Hum Mol Genet*
967 **2018**, *27*, 780–798, doi:10.1093/hmg/ddx440.

968 108. Schwenk, B.M.; Lang, C.M.; Hogl, S.; Tahirovic, S.; Orozco, D.; Rentzsch, K.;
969 Lichtenthaler, S.F.; Hoogenraad, C.C.; Capell, A.; Haass, C.; et al. The FTLD Risk
970 Factor TMEM106B and MAP6 Control Dendritic Trafficking of Lysosomes. *EMBO*
971 *J* **2013**, *33*, n/a-n/a, doi:10.1002/embj.201385857.

972 109. Gory-Fauré, S.; Windscheid, V.; Brocard, J.; Montessuit, S.; Tsutsumi, R.; Denarier,
973 E.; Fukata, Y.; Bosc, C.; Delaroche, J.; Collomb, N.; et al. Non-Microtubular
974 Localizations of Microtubule-Associated Protein 6 (MAP6). *PLoS One* **2014**, *9*,
975 e114905, doi:10.1371/journal.pone.0114905.

976 110. Tortosa, E.; Adolfs, Y.; Fukata, M.; Pasterkamp, R.J.; Kapitein, L.C.; Hoogenraad,
977 C.C. Dynamic Palmitoylation Targets MAP6 to the Axon to Promote Microtubule
978 Stabilization during Neuronal Polarization. *Neuron* **2017**, *94*, 809-825.e7,
979 doi:10.1016/j.neuron.2017.04.042.

980 111. Lu, Q.; Insinna, C.; Ott, C.; Stauffer, J.; Pintado, P.A.; Rahajeng, J.; Baxa, U.; Walia,
981 V.; Cuenca, A.; Hwang, Y.S.; et al. Early Steps in Primary Cilium Assembly
982 Require EHD1/EHD3-Dependent Ciliary Vesicle Formation. *Nature Cell Biology*
983 *2014 17:3* **2015**, *17*, 228–240, doi:10.1038/ncb3109.

984 112. Lee, J.; Chung, Y.D. Ciliary Subcompartments: How Are They Established and
985 What Are Their Functions? *BMB Rep* **2015**, *48*, 380–387,
986 doi:10.5483/BMBRep.2015.48.7.084.

987 113. Gui, M.; Farley, H.; Anujan, P.; Anderson, J.R.; Maxwell, D.W.; Whitchurch, J.B.;
988 Botsch, J.J.; Qiu, T.; Meleppattu, S.; Singh, S.K.; et al. De Novo Identification of
989 Mammalian Ciliary Motility Proteins Using Cryo-EM. *Cell* **2021**, *184*, 5791-
990 5806.e19, doi:10.1016/j.cell.2021.10.007.

991 114. Lagziel, A.; Ahmed, Z.M.; Schultz, J.M.; Morell, R.J.; Belyantseva, I.A.; Friedman,
992 T.B. Spatiotemporal Pattern and Isoforms of Cadherin 23 in Wild Type and Waltzer
993 Mice during Inner Ear Hair Cell Development. *Dev Biol* **2005**, *280*, 295–306,
994 doi:10.1016/j.ydbio.2005.01.015.

995 115. Nicolson, T.; Rüsch, A.; Friedrich, R.W.; Granato, M.; Ruppersberg, J.P.; Nüsslein-
996 Volhard, C. Genetic Analysis of Vertebrate Sensory Hair Cell Mechanosensation:

997 The Zebrafish Circler Mutants. *Neuron* **1998**, *20*, 271–283, doi:10.1016/S0896-
998 6273(00)80455-9.

999 116. Lanford, P.J.; Lan, Y.; Jiang, R.; Lindsell, C.; Weinmaster, G.; Gridley, T.; Kelley,
1000 M.W. Notch Signalling Pathway Mediates Hair Cell Development in Mammalian
1001 Cochlea. *Nature Genetics 1999 21:3* **1999**, *21*, 289–292, doi:10.1038/6804.

1002 117. Zine, A.; van de Water, T.R.; de Ribaupierre, F. Notch Signaling Regulates the
1003 Pattern of Auditory Hair Cell Differentiation in Mammals. *Development* **2000**, *127*,
1004 3373–3383, doi:10.1242/dev.127.15.3373.

1005 118. Bowl, M.R.; Brown, S.D.M. Genetic Landscape of Auditory Dysfunction. *Hum Mol*
1006 *Genet* **2018**, *27*, R130–R135, doi:10.1093/hmg/ddy158.

1007 119. Groza, T.; Gomez, F.L.; Mashhadi, H.H.; Muñoz-Fuentes, V.; Gunes, O.; Wilson,
1008 R.; Cacheiro, P.; Frost, A.; Keskivali-Bond, P.; Vardal, B.; et al. The International
1009 Mouse Phenotyping Consortium: Comprehensive Knockout Phenotyping
1010 Underpinning the Study of Human Disease. *Nucleic Acids Res* **2022**,
1011 doi:10.1093/nar/gkac972.

1012 120. Kolla, L.; Kelly, M.C.; Mann, Z.F.; Anaya-Rocha, A.; Ellis, K.; Lemons, A.;
1013 Palermo, A.T.; So, K.S.; Mays, J.C.; Orvis, J.; et al. Characterization of the
1014 Development of the Mouse Cochlear Epithelium at the Single Cell Level. *Nature*
1015 *Communications 2020 11:1* **2020**, *11*, 1–16, doi:10.1038/s41467-020-16113-y.

1016 121. Kubota, M.; Scheibinger, M.; Jan, T.A.; Heller, S. Greater Epithelial Ridge Cells
1017 Are the Principal Organoid-Forming Progenitors of the Mouse Cochlea. *Cell Rep*
1018 **2021**, *34*, 108646, doi:10.1016/j.celrep.2020.108646.

1019 122. Steiner, A.B.; Kim, T.; Cabot, V.; Hudspeth, A.J. Dynamic Gene Expression by
1020 Putative Hair-Cell Progenitors during Regeneration in the Zebrafish Lateral Line.
1021 *Proc Natl Acad Sci U S A* **2014**, *111*, E1393-401, doi:10.1073/pnas.1318692111.

1022 123. Liu, Y.; Pathak, N.; Kramer-Zucker, A.; Drummond, I.A. Notch Signaling Controls
1023 the Differentiation of Transporting Epithelia and Multiciliated Cells in the Zebrafish
1024 Pronephros. *Development* **2007**, *134*, 1111–1122, doi:10.1242/dev.02806.

1025 124. Hsu, C.-C.; Hou, M.-F.; Hong, J.-R.; Wu, J.-L.; Her, G.M. Inducible Male Infertility
1026 by Targeted Cell Ablation in Zebrafish Testis. *Mar Biotechnol (NY)* **2010**, *12*, 466–
1027 478, doi:10.1007/s10126-009-9248-4.

1028
1029

7. Supplemental Figures

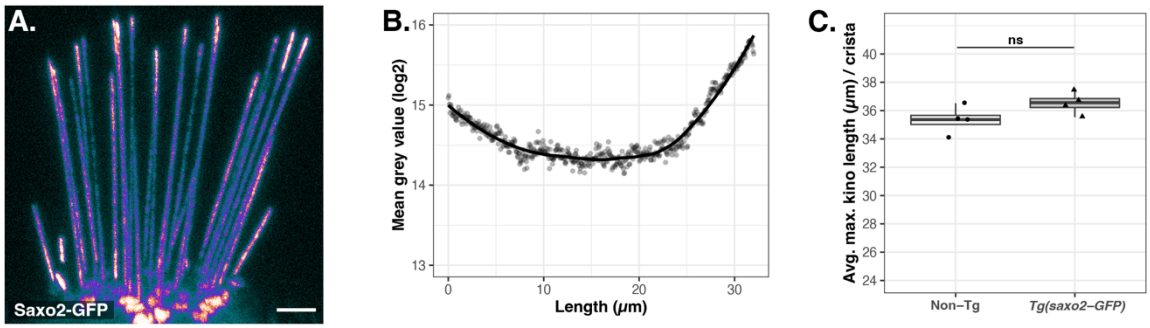

Figure S1. Saxo2-GFP kinocilial distribution and effect on kinocilia height. **A.** Pixel intensity-encoded image of Saxo2-GFP in the kinocilia of lateral cristae hair cells. Brighter colours indicate higher fluorescence intensity. **B.** Scatter plot of averaged mean grey values (log2) for fluorescence intensity from kinocilia in the lateral cristae of 5 dpf Saxo2-GFP transgenics (n = 16 kinocilia from 4 individuals). Position 0 µm is from the proximal region near the base of kinocilia and position 32 µm is the distal-most tip. **C.** Boxplots of maximum kinocilia length in the lateral crista of 5 dpf *saxo2-GFP* transgenics and their non-transgenic siblings. Data points are the average length of the five tallest kinocilia from an individual larva. Two-tailed Welch's t-test statistics: non-Tg, n = 4 larvae, mean = 35.3 µm; *Tg(saxo2-GFP)*, n = 4, mean = 36.5 µm; t = -1.8712, df = 5.5674, p = 0.1143. Scale bar is 5 µm in A.

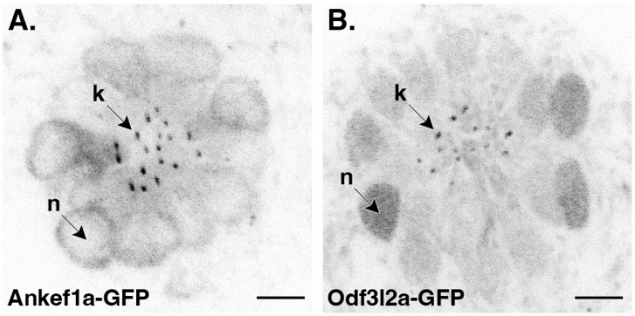

Figure S2. Ankef1a-GFP (**A**) and Odf3l2a-GFP (**B**) localization patterns in the soma of neuromast hair cells (top-down views). n = nucleus, k = kinocilium. Scale bars are 5 µm.

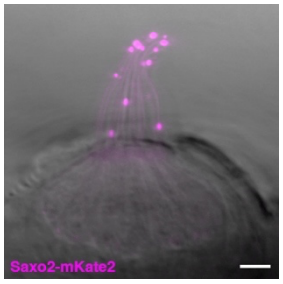

Figure S3. An example of truncated and bulbed kinocilia in the neuromasts of *saxo2-mKate2* transgenics with the "severe" overexpression phenotype. Scale bar is 5 µm.

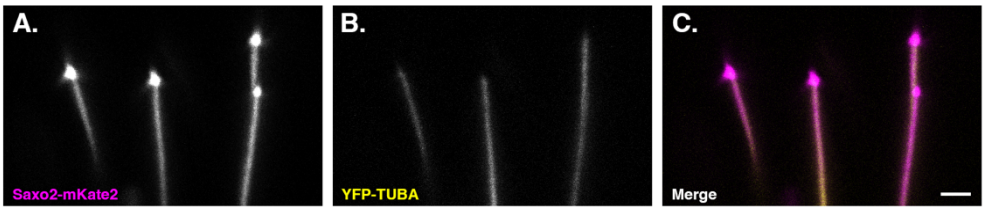

Figure S4. Detail of Saxo2-mKate2 (**A**) and YFP-TUBA (**B**) co-expression at the distal tip of kinocilia in the lateral cristae. Merged channels are shown in C. Scale bar is 2 µm.

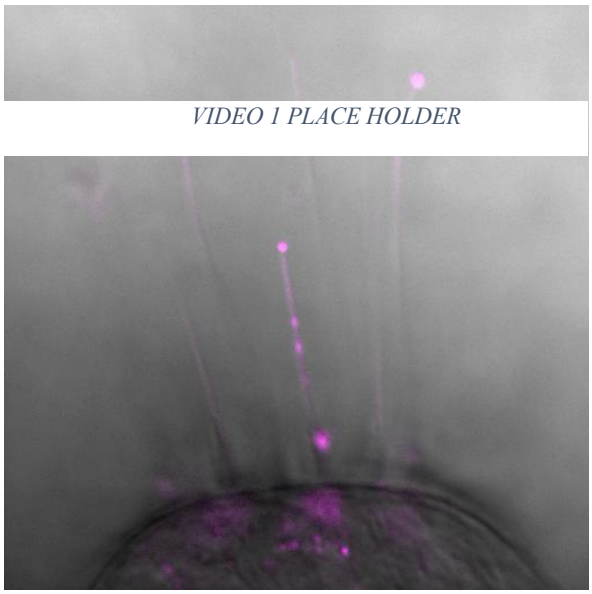

Video S1. Bidirectional movement of a Saxo2-mKate2 positive puncta in the kinocilium of a lateral crista hair cell in a 5 dpf zebrafish larva.